# Combine ligand and structure based methodologies to probe stereo-selectivity of CYP3A4 inhibitors


**By**

**Sadia Mukhtar**

**NUST201361541MRCMS64213F**

**Research Center for Modeling and Simulation**
**National University of Sciences & Technology**
**Islamabad, Pakistan**
**2015**

# Combine ligand and structure based methodologies to probe stereo-selectivity of CYP3A4 inhibitors

**By**

**Sadia Mukhtar**

**NUST201361541MRCMS64213F**

A thesis submitted in partial fulfillment of the requirement for the degree of

Masters in Computational Sciences and Engineering

With

Majors in Bioinformatics

**Research Center for Modeling and Simulation**
**National University of Sciences & Technology**
**Islamabad, Pakistan**
**2015**

## TH4 page

# Statement of Originality

I hereby declare that this thesis comprises of my own effort and research work and none of its contents are plagiarized or submitted to other universities. The contributions of different people in this work is acknowledged and duly referenced.

Sadia Mukhtar
NUST201361541MRCMS64213F

# Acknowledgement

First of all I want to thanks my Allah (S.W.T) for blessing me with opportunity to learn and grow in this world of knowledge and wisdom. I want to convey my gratitude to my respected supervisor Dr. Ishrat Jabeen for her support, guidance and encouragement throughout the whole tenure. Her dedication, keen knowledge on the subject and fortitudes were a great source of motivation for me to put in my best efforts for the completion of the project.

I also want to thank Research Centre for Modelling and Simulation (RCMS) for providing me with various facilities and assistance whenever needed. I appreciate the support of my Graduation Examination Committee (GEC): Dr. Jamil Ahmad, Dr. Farooq Ahmad Kiani, and Dr. Amjad Ali who provided me with best atmosphere to learn and achieve the required objectives which without their support would have been formidable.

I owe my sincere gratitude to my colleagues and friends at Pharmacoinformatics Lab, Noreen Akhtar, Saba Munawar, Sadia Zafar, Mehrin Gul (Late), Yusra Sajid Kiani, Raheel Khan, and Sara Azhar, for providing the best working atmosphere. Furthermore, I want to acknowledge my colleagues and batch mates i.e. Aneeqa Arshad, Hira Ejaz, Zunaira Rauf and Fareha Tahir. I would also like to say thanks to my family whose continuous backing was a great source of inspiration and motivation for me throughout the tenure.

# Dedication

**I dedicate my work to**
**My beloved Family**

# Table of Content

# List of Abbreviations

| | |
|---|---|
| ADMET | Absorption, Distribution, Metabolism, Elimination and Toxicity |
| CYP-P450 | Cytochrome-P450 |
| CYP3A4 | Cytochrome-P450 3A4 |
| SRS | Substrate Recognition Site |
| NADPH | Nicotinamide Adenine Dinucleotide Phosphate |
| QSAR | Quantitative Structure Activity Relationship |
| PDB | Protein Data Bank |
| RMSD | Root Mean Square Deviation |
| 2D | 2 Dimensional |
| 3D | 3 Dimensional |
| HBA | Hydrogen Bond Acceptor |
| HBD | Hydrogen Bond Donor |
| GA | Genetic Algorithm |
| PLS | Partial Least Squares Method |
| GRIND | GRID Independent Molecular Descriptors |
| SVM | Support Vector Machine |
| SAR | Structure Activity Relationship |
| CoMFA | Comparative Molecular Field Analysis |
| CoMSIA | Comparative Molecular Similarity Indices Analysis |
| ANN | Artificial Neural Network |
| cLogP | Calculated LogP |
| $IC_{50}$ | Inhibitory Concentration 50 |
| $pIC_{50}$ | Log of $IC_{50}$ |

| | |
|---|---|
| LipE | Lipophilic Efficiency |
| ADME | Adsorption, Distribution, Metabolism, Excretion |
| MIF | Molecular Interaction Field |
| MOE | Molecular Operating Environment |
| CLACC | Consistently Large Auto And Cross Correlogram |
| FFD | Fractional Factorial Design |

# List of Figures

## Figure number Caption Page no

# List of Tables

## Table no Caption Page no

# Abstract

Cytochrome P450 (CYP-P450) enzymes play critical role in the metabolic processes of the body. These microsomal proteins are involved in the breakdown and detoxification of various xenobiotics, nutrients and clinically administered drugs. The CYP3A family is the largest subfamily of the CYP isoforms in the liver. There are at least four isoforms including 3A4, 3A5, 3A7 and 3A43 of which 3A4 is the most abundant hepatic microsomal enzyme involved in the drug metabolism. Several drugs have tendency to inhibit the normal physiological functioning of CYP3A4 with varying potencies thus, resulting in varying toxic effects. In a quest to avoid CYP3A4 inhibition related drug toxicity, various studies reported the 3D interaction patterns of the CYP3A4 inhibitors and substrates. However, until now no report about molecular level interaction of stereoisomeric drugs with CYP3A4 is available. Since these interactions takes place in asymmetric space, overlooking the stereochemistry of the ligands can compromise the accuracy of various *in silico* structure based methodologies. Therefore, a detailed knowledge about 3D structural features important for the inhibition of CYP3A4 and stereoselectivity of its inhibitors are noteworthy for analysis. *In silico* approaches for predicting CYP inhibition potential of stereoisomeric drugs are lucrative as they may be applied to whole set of chemical libraries at the outset of the drug discovery process, usually at very small cost investment at in vivo level. In that way, the *in silico* models offer considerable potential for reducing the number of experimental studies required for compound selection and for improving the success rate. Therefore, in this project we employed both structure based and ligand based *in silico* methods to explore the stereo-selectivity as well as ligand interaction profiles of CYP3A4 stereo-isomeric inhibitors. Difference between interaction patterns of stereoisomers of CYP3A4 inhibitors was analyzed, which was further reinforced by building GRIND model for analysis of difference in 3D

structural features among isomeric pairs of CYP3A4 inhibitors. Our results demonstrate that the difference in inhibitory potency of different stereoisomeric pairs is because of difference in their interaction pattern within the binding cavity of CYP3A4. 3D structural features that contribute significantly in inhibition are two hydrophobic features at a distance of 12.0 to 12.40Å. The 3D interaction based differentiating features between stereoisomers include two hydrogen bond acceptors at a distance of 16.80 to 17.20Å and one hydrogen bond acceptor and a hydrophobic region at a distance of 18.40 to 18.80Å. Similarly, a hydrogen bond donor and a hydrogen bond acceptor at a distance of about 8.80 to 9.20Å are present in S isomers while absent in R isomeric form of CYP3A4 inhibitors. These results could pave the way towards safer drug development.

***Chapter 1***

# Introduction

Most common cause of failure of newly developed drug entities in clinical trials is their poor pharmacokinetic/ADME-TOX (absorption, distribution, metabolism, elimination and toxicity) parameters and/or the lack of efficacy [1]. Similarly, drug toxicity induced by drug-drug and drug-nutrient interactions are mainly due to poor drug metabolism and thus, is one of the very important factors in the drug failure. Therefore, in order to minimize the drug failure rate in later stages of investigation, pharmacokinetic properties of the drugs in general and metabolism in particular should be focused along with their efficacy [2]. Drugs are metabolized and eliminated from the body in two different phases namely Phase 1 and Phase 2 [3].

In phase 1 metabolism cytochrome-P450 (CYP-P450) metabolizing enzymes convert lipophilic drugs in to easily eliminated and less toxic hydrophilic compounds while in phase 2 conjugation reactions takes place [3]. CYP-P450 enzymes is a super-family of heme-containing proteins that comprise of about 57 members in human genome having various isoforms on the basis of difference in their amino acid sequence [4]. CYP-P450 enzymes are not only critical for metabolism of drugs but also play important role in biotransformation of xenobiotic and detoxification of poisonous compounds [5]. The key P450 enzymes that participate in 90% metabolism of clinically administered drugs are CYP1A2, CYP2C9, CYP2C18, CYP2C19, CYP2D6, CYP2A6, CYP2E1 and CYP3A4 [6-10]. Inhibition or induction of these enzymes result in toxicity and Drug-drug interactions due to unpredictable drug concentration in human body[11].

CYP3A4 is most important and abundant enzyme in the human body that metabolizes more than 60% of clinically administered drugs. Thus, it shows that CYP3A4 enzyme has low substrate selectivity that results in making this enzyme more susceptible to various inhibitors thus, resulting in both reversible and irreversible inhibition by structurally diverse set of drugs [12]. This inhibition is either due to chemical alteration of the heme present in CYP3A4 enzyme, changes in the protein or due to covalent binding of altered heme to the enzyme protein [13].

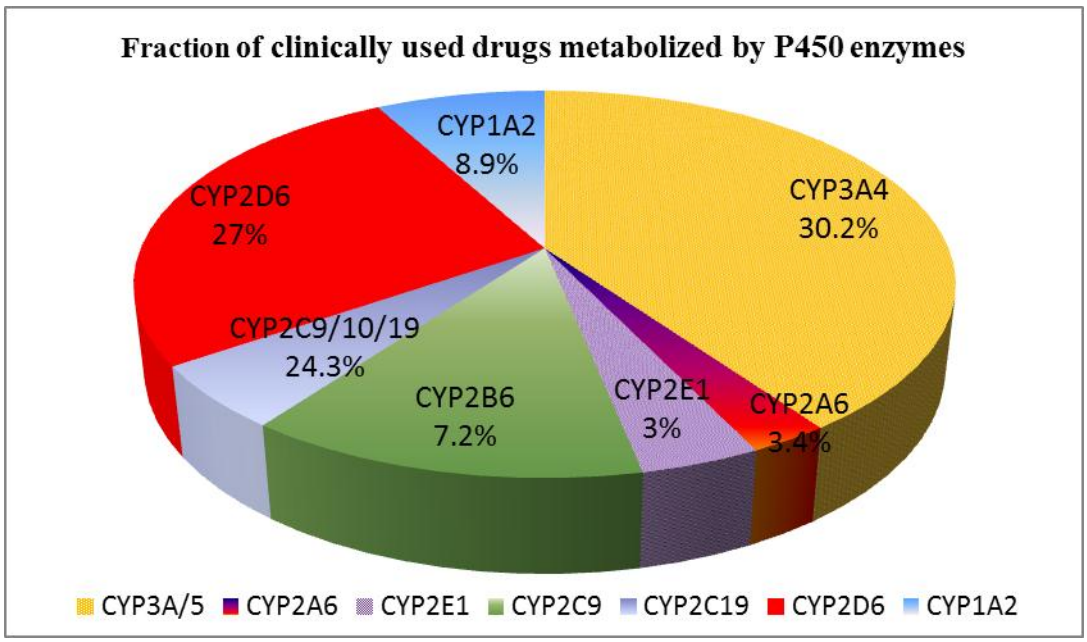


**Figure 1**: Pie chart representing fraction of clinically used drugs metabolized by P450 isoforms (modified from [14])

CYP3A4 like all other mono-oxgenases is a membrane bound protein. Separation of the protein from the lipid bilayer leads to exposure of hydrophobic surfaces that have a tendency to associate nonspecifically [15]. CYP3A4 preserves the common tertiary structure formerly analyzed for other P450s, which consists of various α helices and β sheets that are recognized with A to L alphabets [16]. The core of P450s that is conserved comprises of a bundle of four helices that are D, E, I, and L and additional J and K helices. In addition to these helices two sets of sheets are also present that are structurally conserved which helps to create a path for hydrophobic compounds to access [17]. The regions that are not conserved

consist of A, B, F and G helices. These regions are involved in binding of substrate in the active site [17].

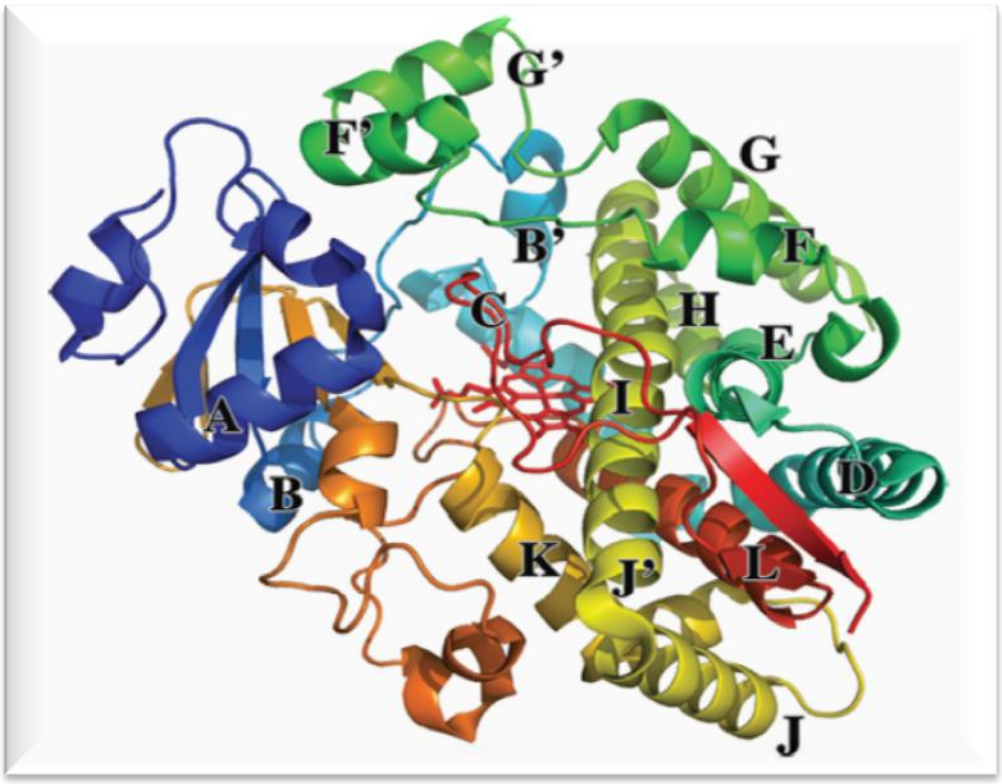


**Figure 2:** General structure for the CYP isoforms depicted by the CYP3A4 pdb ID 3NXU showing the helical structures labeled from A to L [18, 19].

The SRS-1 (Substrate Recognition Site) comprises of loops BB′ and B′C while SRS-2 and SRS-3 CONSIST of loops formed by F and G and their helices [20]. SRS-4 is conserved region having helix I. The protruding end of β4 sheet forms the SRS-6 region while SRS-5 consist of the β-sheets from 1 to 4 and the N terminus of the protein [20]. The alpha and beta domains are shown in figure 3 which is also depicting differentiating structural properties of CYP3A4 enzyme from other isoforms.

In CYP3A4 crystal structures the F and G helices are shorter as compared to typical P450 structures. Two helical segments are present in FG loop. A distinctive phenylalanine cluster is present in CYP3A4 active site formed by interaction of three phenylalanine residues from linker region with F and I helices as well as BC region [16, 21]. Most common regions involved in interaction at the active site are N terminal that is end of helix A, BC loop, helix I

and some portion of β3 and β5 sheets [16, 21]. The inhibitors interact with the active site of CYP3A4 near the heme group that is at the floor of the active site and usually occupies only a part of the binding cavity. The conformational modification takes place in F and G helices when CYP3A4 binds with a ligand. The clusters of phenylalanine residues are also opened and some of the hydrophobic residues are exposed in the vicinity of the active site. The amino acids Arg-212 and Leu-211 that are present on the surface in ligand free structures are directed inside the binding pocked in case of ligand bounded CYP3A4 enzyme. While, in case of substrates like erythromycin the most prominent changes are observed in F and G region [22].

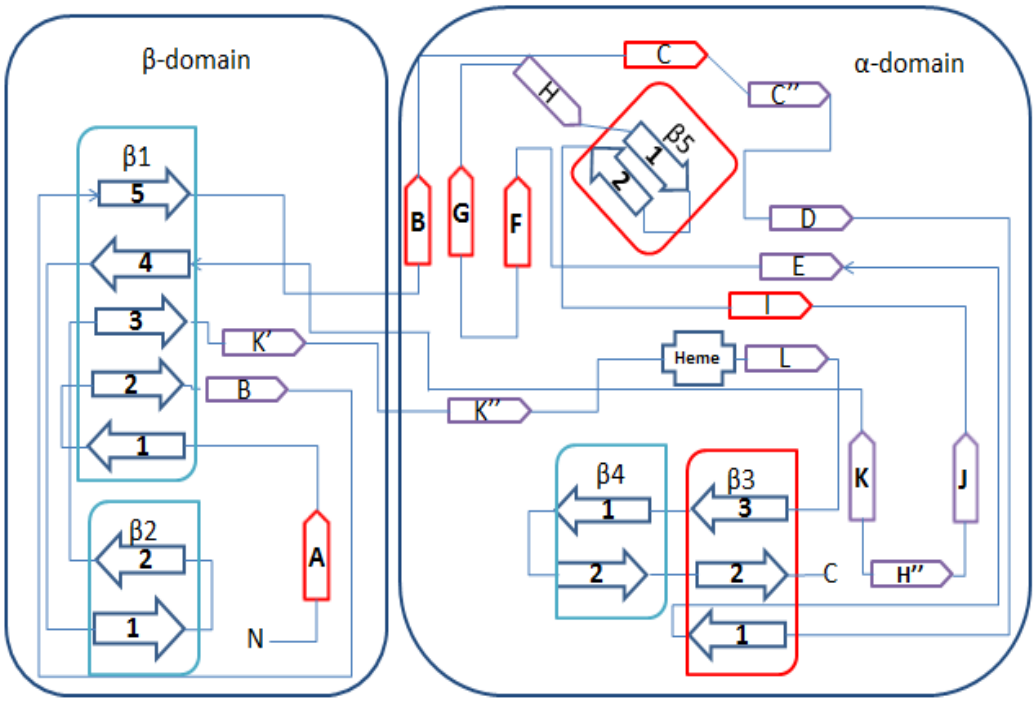


**Figure 3**: The above figure is elucidating the secondary structural parts of P450 enzymes. The purple or red (in case of CYP3A4) pentagons are representing helices. The arrows are representing the sheets while the blue lines are representing random coils. The regions highlighted in red are differentiating structural features of CYP3A4 from other CYP-P450 enzymes. The alpha and beta domains are also highlighted. The above illustration is a reformed demonstration of CYP-P450 enzyme structural features which was taken from Peterson and Graham [20].

A general catalytic mechanism for the oxidation reaction is initiated by binding of substrate with P450 enzyme which also results in conformational changes in the enzyme. In the next step electron is transferred from Nicotinamide adenine dinucleotide phosphate (NADPH) facilitated either by cytochrome P450 reductase or other related reductase resulting in the reduction of heme group from ferric ($Fe^{+3}$) to ferrous ($Fe^{+2}$) state. In third step molecular oxygen is bounded to heme ($Fe^{+2}$) iron which is followed by the further reduction of enzyme-substrate complex by transfer of second electron. In fifth step water is released and activated oxygen intermediate is produced. In second last step the oxygenated product is released which is followed by recovery of initial heme-protein enzyme complex along with return of water molecule to occupy distal coordination position of iron nucleus. [23]. All the steps are shown in the following figure 4 [23].

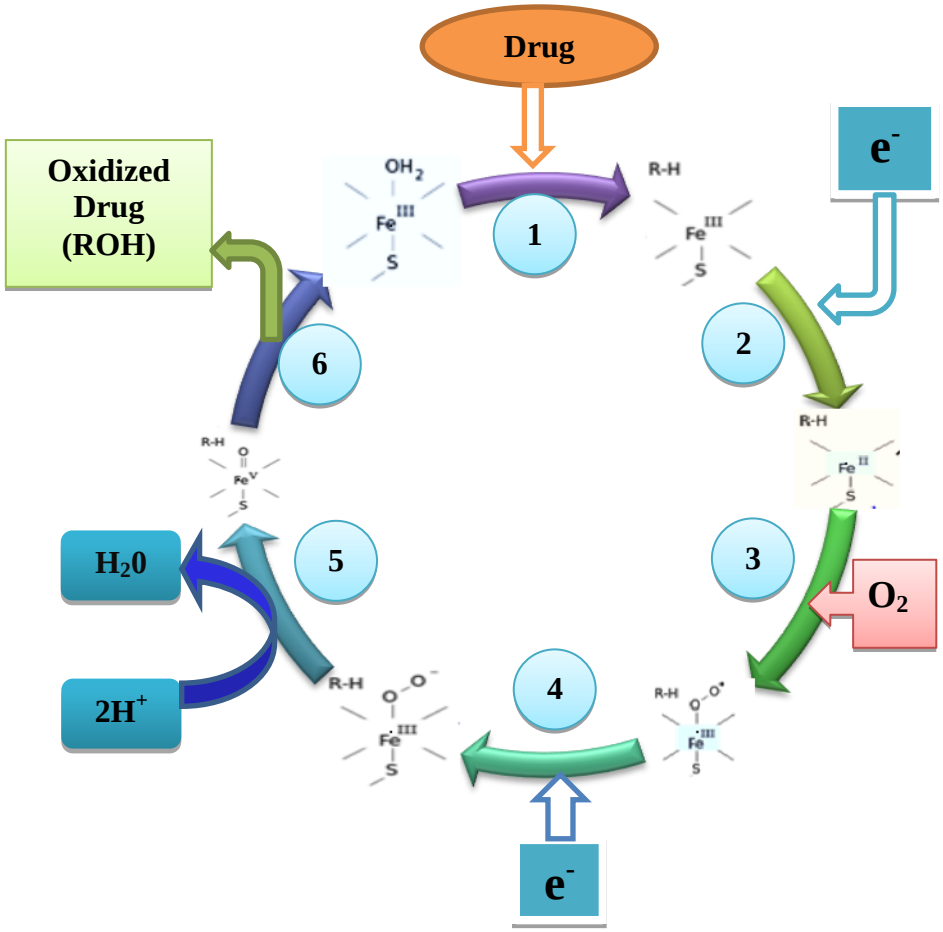


**Figure 4:** The catalytic cycle of cytochrome P450s (Changed and modified from [23]).

CYP3A4 enzyme has most promiscuous binding site among heme containing P450s [24]. Inhibition of CYP3A4 by structurally and functionally diverse compounds is one of the major reason of unwanted drug-drug interactions[24]. The most important CYP3A4 inhibitors include antibacterial, calcium channel blockers [24], anti HIV agents (e.g. ritonavir), antihypertensive, steroids and their modulators (e.g. gestodene and raloxifene), quite a few herbal constituents (e.g. hypericin. Hyperforin, biapigenin) and some supplements [25-27]. Inhibition of CYP3A4 results in either toxic or suboptimal therapeutic outcome. Although experimental evaluation of new drugs against CYP3A4 enzyme is done but all new drug molecules cannot be evaluated by experimental techniques due to high cost and also because the procedures are time consuming [28].

*In silico* approaches are vital to evaluate new drug molecules [29]. Abundant *in silico* techniques are available to predict ADMET properties of compounds that encompass ligand based methods quantitative structure activity relationship (QSAR), 2D-QSAR, 3D-QSAR, as well as structure based methods consisting of ligand-protein interactions, docking and pharmacophore modeling [30, 31]. Statistical regression technique such as PLS (partial least square) that is applicable for predicting linear models correlating structural properties and their activities. Classification models are built when direct correlation between activity and descriptors does not exist or complex biological mechanisms are involved in defining certain ADMET property. Classification tools include support vector machines, decision trees and k-nearest neighbor. Artificial neural networks and genetic algorithm are additional tools that aid in development of reliable models for ADMET predictions [32, 33]. ADMET properties are influenced by interactions between drug entities and molecular systems which can be analyzed using quantum mechanics and molecular mechanics simulations [34].

Several pharmaco-informatic strategies to investigate substrate\inhibitor binding to CYP-P450 have demonstrated that these interactions are complex, multi-site and conformation sensitive processes. Since these interactions take place in three-dimensional and asymmetric space thus, ignoring the stereoselectivity associated with small molecule–transporter binding only complicates and reduces the accuracy of the QSAR and other modeling analyses [35].Regardless of the fact that various QSAR models and docking studies are available for CYP3A4 inhibitors [36, 37]. In all these studies stereoisomerism of the compounds are not considered and racemates of these compounds are used. However, in most of the racemates one enantiomer might have different inhibitory potency for CYP3A4 as compared to the other stereoisomer. This is might be due to difference in their potential binding pattern. Therefore, in this project we used both structure based and ligand based *in silico* methods for investigation and exploration of stereselectivity as well as ligand interaction profiles of CYP3A4 stereoisomeric inhibitors. Specific 3D structural features involved in the inhibition of this enzyme have been identified by several ligand based strategies that adds value towards molecular basis of drug metabolism and to avoid unwanted drug-drug interaction.

**Objectives of the study:**

1. General goal of this study is to correlate the difference in biological activity of different stereoisomeric pairs with their interaction pattern as well as with their ease of transport.
2. Study of interaction profile of different stereo-isomeric CYP3A4 inhibitors.
3. Identification of special pharmacophoric features involved in inhibition of CYP3A4.
4. Developing reliable models using both structure based and ligand based *in silico* methods to predict CYP3A4 inhibition potencies of new drug entities.

***Chapter 2***

# Literature review

Cytochrome P450 (P450s) are superfamily of enzymes consisting of heme. Cytochrome P450s were first identified by Martin Klingenberg (1958). In this study the spectrophotometric analysis of the pigments present in the microsomal fraction extracted from rat livers was conducted in which absorbance at specific wavelength 450 was detected, thus, resulting in nomenclature of cytochromes as P450s [38]. The superfamily is further classified into families depending upon the pairwise identity in the amino acid sequence among distinct members that should be >40%, and then further division into subfamilies provided that the pairwise amino acid sequence identity is ≥55% [39]. CYP3A4 is the major enzyme involved in drug metabolism due to its abundance in human body, large active site and its ability to deal accommodate with more than one drugs in its binding pocket at a time [40, 41]. Therefore, it is crucially imperative for the medicinal industries involved in the development of new drugs to be competent enough to predict in initial stages that how a drug molecule will interact with cytochromeP450 family in general and with CYP3A4 in particular. Therefore, that whether that drug candidate is good enough for spending time and money to take through further experimentation or that the drug candidate will fail due to drug-drug interactions and toxicity [42]. *In silico* structure based and ligand based approaches to foresee ADMET properties of drugs are commonly employed nowadays.

## 2.1 Structure based approaches:

### 2.1.1 CYP3A4 structure:

Several studies are available on CYP3A4 crystal structure explaining its conformations and its interactions with various inhibitors and substrates. In P450s there are

certain domains in the structures that are conserved in all cytochrome P450 enzymes. These domains include E, I, J, K, L helices and along with portions of β -1 sheet that form the core of P450 proteins. These preserved portions make a conserved binding site for the prosthetic group heme along with the cysteine residue that is an axial ligand to that heme moiety [43]. In CYP3A4 structure there is an additional helix present at the end of N terminus but its function is not clear. Furthermore, CYP3A4 differ in other regions those are BC and FG helices. The F and G helices are shorter in CYP3A4 [16].

**Table 1:** Crystal structures available in protein data bank of CYP3A4

| CYP isoform | Pdb ID | Source | Ligand bound | Chains | Resolution Å | Year | Refer-ence |
|---|---|---|---|---|---|---|---|
| CYP3A4 | 1TQN | Homo sapeins | Erythromycin | A | 2.05 | 2004 | [44] |
| CYP3A4 | 1W0E | Homo sapeins | Metyrapone and progesterone | A | 2.80 | 2004 | [45] |
| CYP3A4 | 1W0F | Homo sapeins | Metyrapone and progesterone | A | 2.65 | 2004 | [45] |
| CYP3A4 | 1W0G | Homo sapeins | Metyrapone and progesterone | A | 2.73 | 2004 | [45] |
| CYP3A4 | 2J0D | Homo sapeins | Ketoconazole and erythromycin | A,B | 2.75 | 2006 | [22] |
| CYP3A4 | 2V0M | Homo sapeins | Ketoconazole and erythromycin | A,B,C,D | 2.80 | 2006 | [22] |
| CYP3A4 | 3NXU | Homo sapeins | Ritonavir | A,B | 2.00 | 2010 | [46] |
| CYP3A4 | 4I4H | Homo sapeins | Three Desoxyritonavir analogues | A | 2.90 | 2013 | [47] |
| CYP3A4 | 4I4G | Homo sapeins | Three Desoxyritonavir analogues | A | 2.72 | 2013 | [47] |
| CYP3A4 | 3UA1 | Homo | Bromoergocry-ptine | A | 2.15 | 2012 | [48] |

| | | | | | | | |
|---|---|---|---|---|---|---|---|
| | | sapeins | (BEC) | | | | |
| CYP3A4 | 3TJS | Homo sapeins | Ritonavir analogs | A | 2.50 | 2012 | [49] |
| CYP3A4 | 4K9T | Homo sapeins | Desoxyritonavir analogues | A | 2.50 | 2013 | [50] |
| CYP3A4 | 4K9V | Homo sapeins | Desoxyritonavir analogues | A | 2.60 | 2013 | [50] |
| CYP3A4 | 4K9X | Homo sapeins | Desoxyritonavir analogues | A | 2.76 | 2013 | [50] |
| CYP3A4 | 4K9W | Homo sapeins | Desoxyritonavir analogues | A | 2.40 | 2013 | [50] |
| CYP3A4 | 4K9U | Homo sapeins | Desoxyritonavir analogues | A | 2.85 | 2013 | [50] |
| CYP3A4 | 4I3Q | Homo sapeins | Three Desoxyritonavir analogues | A | 2.60 | 2013 | [47] |

CYP3A4 both ligands bounded and non-ligand bonded crystal structures are available, comparison of ketoconazole bounded structure and ligand free structure having pdb ID 2VOM and 1TQN respectively revealed the RMSD of about 1.60 Å for all Cα atoms. The difference in these structures was in the conformational changes in the helices F and G. The most prominent conformational changes are seen in helices along with the intervening loops. The phenyl alanine moieties cluster that is distinct for CYP3A4 enzyme is fragmented in ligand bound enzyme, resulting in exposure of hydrophobic side chains in the surrounding media [22]. The residues 210-213 adopt a helix like structure in ligand bound enzymes which usually lack secondary structural form in non-ligand bounded enzyme [22]. Another difference between ligand bounded and ligand free structures is the position of Arg-212. In Yano, *et al*, the side chain is positioned towards the heme iron in which the enzyme is in apostate while in Williams *et al*. in which the enzyme is ligand bounded this residue is

rotated at an angle of about $120^0$ and is positioned away from heme moiety [44, 45]. Arg-212 moiety is present on the surface of protein structure when CYP3A4 complexes with ketoconazole, this disparity of Arg-212 residue among different CYP3A4 crystal structure shows flexibility in enzyme structure as well as the binding cavity [22].

### 2.1.2 Active site of CYP3A4:

CYP3A4 metabolizes diverse nature of substrates and the active site of CYP3A4 is known to accommodate more than one substrates of small size at a time or large ligands due to homotropic and heterotropic cooperativity of the enzyme [16]. CYP3A4 shows positive homotropic cooperativity which means that as the ligands bind at the active site of the enzyme the affinity of the enzyme for the ligands will increases. It is observed in previous studies that the homotropic cooperativity is decreased due to substitution of Leu-211 residue with phenylalanine residue [51]. Heterotropic cooperativity is enhancement of CYP3A4 activity due to interaction of effectors like α-naphthoflavone at the effector site consequently increasing rate of substrate metabolism. The heterotropic cooperativity might be clinically noteworthy due to its role in drug-drug interactions [52]. The kinetics of CYP3A4 for drug metabolism shows non-Michaelis–Menten behavior that is either due more than one substrate binding sites or due to kinetically different conformers. In evidence of available information it is predicted that none of these two explanations can be omitted and even it is proposed that both of these mechanisms work simultaneously [22, 53, 54].

### 2.1.3 Docking Studies:

Molecular docking studies have been conducted by several authors. These studies are employed to classify and improve drug candidates by inspecting molecular interactions among ligands and the target macromolecules. The catalytic site of CYP3A4 has been explored using techniques like site directed mutagenesis, methods including X-ray

crystallography, protein modeling and docking studies. Important interacting site amino acid residues extracted from these studies include Asp-217, Asn-104, Arg-105 and 212, Ser-119 and 478, Glu-374, Met-114, Asp-214, Ile-301 and 369, Ala-305 and 370, Pro218, Leu211, 373 and 479, Thr309, Phe-108, 219, 220, 241, 215 and Phe-304 [44, 45, 55-57].

In order to shed light on 3D ligand-protein interaction pattern, a number of docking studies have been performed using compounds of diverse nature into ligand bounded and ligand free X-ray crystal structures of CYP3A4 having PDB IDs 1W0E, 1W0F, and 1W0G described by Williams, *et al*. In one of these studies metyrapone is docked in CYP3A4 and its interaction with active site are analyzed. In this study Ser119 was found interacting with carbonyl group of metyrapone and it stabilizes the inhibitor enzyme complex, while pyridinyl group interact directly with heme of the enzyme. Additional important amino acids residues involved in interaction between CYP3A4-metyrapone complex are Arg-105, Ile-301, Phe-304, Ala-305, Thr-309 [58]. In another investigation, loperamide interactions with CYP3A4 have been analyzed by docking it in the crystal structure of CYP3A4 having PDB ID1TQN (Yano, *et al*, 2004). It was reported that loperamide interacts with CYP3A4 via polar and non-polar interactions involving Arg-212, Glu-374 amino acids and phenyl alanine hydrophobic cluster respectively [59]. Further**,** Jayakanthan, *et al,* explored interaction between ten HIV-protease drugs and CYP3A4 and identified that important drug binding amino acids were Ser-119, Ala-370, Glu-374, and Arg-105, 106, 212 and 372 in addition to heme and phenylalanine clusters. Crystal structure of CYP3A4 having PDB ID 1TQN and resolution 2.05Å was used. The results of this study were consistent with data already obtained from mutagenesis studies, modeling, and docking studies [57]. In another study cytochrome P450 inhibition was investigated against 33 flavonoid derivatives. Six flavones were docked in CYP3A4 enzyme crystal structure having PDB ID 1TQN and following important amino acid residues were extracted Arg105, Arg-106, Phe-108, Leu-210, Arg-212, Ile-301, Phe-304, Ala-305, Glu-308,

Thr-309, Ile-369, Ala-370, Met-371, and Arg-372 [60]. Tanaka and coworkers characterized the binding cavity of CYP3A4 enzyme using homology modeling and it was further docked with inhibitors i.e. losartan and paclitaxel were studied in detail. Significant amino acid residues involved in interaction were Glu374 and two acidic amino acids Asp214 and Asp217 these were present at the distal end of the active site [61]. Lill, *et al*, performed docking and QSAR studies on structurally diverse data set of CYP3A4 inhibitors. The important amino acid involved in ligand-protein interaction comprises Phenylalanine residues including Phe-57, 74, 108, 213 and Phe-215. Other important residues were Ile-120, Val-81, Leu-216, Phe-241, Ile-301, Phe-304, Val-393, Phe-213, Leu-482, Glu-374, and Arg-106. While Arg-106, Arg-212 as well as Arg-372 are involved in hydrogen bonding interactions[62]. Similarly, Ritonavir was docked in crystallized structure having PDB ID 1TQN of CYP3A4 at 2.0Å resolution and its interactions in the binding cavity were discussed. Ritonavir structure has two phenyl rings one of the ring is parallel to the heme and at a distance of 4.0 Å, while other is surrounded by hydrophobic amino acids that are by Phe108, Leu210, Leu211, Phe241, Ile301, and Phe304. Vander der Waals interactions are also observed involving Ile369, Ala370, and Leu373 amino acid residues. Other important amino acids were Tyr53, Phe57, Phe213, Phe215 Asp61, Asp76, Arg106, Arg372, an Glu374 that is part of the polar umbrella [46]. Following figure 5 is showing important amino acid residues involved in CYP3A4–inhibitor interactions from various docking studies. In the studies by Lill, *et a.*, and Tanaka, *et al*, the common amino acids include Glu-374 while Asp214 and Asp-217 are observed in the later study only [61]. While in studies by Jayakanthan, *et al*, and Park, *et al*, the amino acids that are overlapping consist of include Arg-105, Phe-304 and Ser-119 [57, [58]. However, the amino acid that was exclusively identified by Jayakanthan, *et al*, is Phe-107 [57]. In the comparison of studies by Shimada, *et al*, and Park, *et al.*, the common amino acids identified in both studies include Arg-105 and 106, Phe-304, Ala-370, Ile-301, Ala-305 and Thr-224,

while, those amino acids that were exclusively involved in interactions in the study by Shimada, *et al*, consist of Leu-210, Glu-308, Ile-369, Met-371 and Arg-372. The amino acids are that are common among more than two docking studies include Arg105, Arg-106, Phe-304 and Glu-374. Few amino acids are unique in individual studies as each study employs different dataset, protein structure, procedure for binding cavity selection and algorithm for docking of the ligands inside the binding cavity.

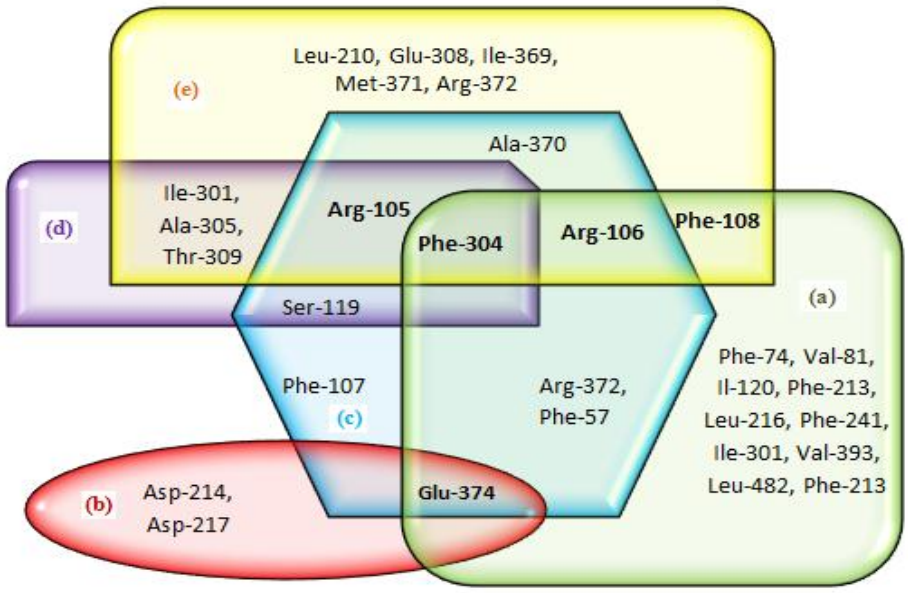


**Figure 5**: Shows comparison of specific and overlapping amino acid residues at CYP3A4 ligand binding site. [62](a-Diverse dataset), [61] (b-Losartan and Paclitexal), [57] (c HIV-protease inhibitors), [58] (d-Metyrapone), [60] (e-Flavones).

### 2.1.4 Homology models of CYP3A4:

In 2001 Dai, *et al*, and his coworkers generated a homology model of human enzyme CYP3A4 [63]. In this study the template structure that was used for modeling was the rabbit P450-2C5 which was solved chimeric structure having PDB ID 1TD6 from the study Williams, *et al*, 2000 [15]. Multiple sequence alignment was utilized to build the model via alignment of solved crystal structure 1TD6 with the sequence of 6 human microsomal enzymes namely CYP3A4, CYP2C9, CYP2C8, CYP2C8, CYP2C18, CYP2C19. In this

model seven small loops having 3 to 9 amino acid residues were generated by the loop generation program available in the package of Molecular Simulations homology program. In the predicted model there were no deletions and Gaps. Therefore, the model was quite reliable. The overlaps and steric bumps were modeled by molecular dynamics [63].

CYP3A4 is the most essential human cytochrome P450 enzyme which contributes in the xenobiotic and drug detoxification. So, CYP3A4 is also involved in major drug-drug interactions. Therefore, in this study by Tanaka, *et al*, for clear understanding of its active site, a homology model of CYP3A4 was built using the coordinates from solved crystal structure of mammalian CYP2C5 [15]. The predicted active site of CYP3A4 is quite large as compared to that of CYP2C5. It was divided into three parts which included a proximal site and two distal sites based on the distance from heme. Amino acid residues that were stated to be significant for ligand-protein interactions were positioned inside the active site of the predicted model. Furthermore, few inhibitors for e.g. paclitaxel were docked into the constructed model. Docking of 14 substrates was conducted by employing the Ph4Dock of MOE. The docking results proposed that the model was consistent and thus can be further used for designing new drug molecules having higher affinity for actual target and lower association with the anti-target CYP3A4 to eradicate the problem of enzyme inhibition [64].

## 2.2 Ligand based studies:

There are several ligand based strategies available that provide information about the active site of protein directly based on electronic properties and conformations of the ligands. However, these models are dependent on the availability of reliable data source of adequately large no of ligands along with their conformations as well as biological activities. Quantitative structure activity relationship (QSAR) in general is a coorelation between the biological activity and their empirical parameters in a quantitative manner. Pharmacophoric models are made on the basis of important features extracted from set of already identified

ligands, the ensemble of these important features that include electronic, steric and hydrophobic as well as aromatic are necessary for optimal interactions of ligands with a specific biological target [42, 65].

### 2.2.1 Pharmacophore based models:

The first QSAR (quantitative structure-activity relationship) model of CYP3A4 ligands was generated by using a diverse dataset of 38 CYP3A4 substrates. Pharmacophoric model was built by employing the program catalyst. Final pharmacophoric model that was obtained comprised of four essential features namely two HBA (hydrogen bond acceptor), one hydrophobic and one HBD (hydrogen bond donor). It was analyzed that CYP3A4 substrates comprising of more than one hydrophobic regions are involved in interaction inside the binding cavity at a site away from the metabolic cavity [66]. In another study of Ekins, *et al.,* and his coworkers pharmacophoric model of CYP3A4 inhibitors was built using program Catalyst. CYP3A4 inhibitors model was built from three sets of data in which three models were trained. Competitive inhibition was studied and Catalyst model was built by using 14 and 32 competitive inhibitors against midazolam 1-hydroxylase and cyclosporine-A hydroxylation respectively. Formerly published data of $K_i$ and $IC_{50}$ values was also employed to construct QSAR models. Most important pharmacophoric features that were extracted to be involved in CYP3A4 inhibition comprises of three hydrophobic groups at distances of 4.2 to 8.8 Å from at least one hydrogen bond acceptor [67].

When we compare above two studies it is observed that with the increase in no of hydrophobic regions overall inhibitory potency of the ligands also increases but hydrogen bond donor feature was observed in substrates only and it was absent in inhibitors pharmacophoric model. However, both the hydrophobic and hydrogen bond acceptor regions are crucial for interaction of both substrates and inhibitors with the enzyme. Row *et al*, synthesized and evaluated 8-geranyloxypsoralen analogues of CYP3A4 inhibitors. It have

been observed in this study that three out of four binding regions reported in Ekins, *et al*, [67] are involved in interaction of these analogues with CYP3A4. One mutual structural feature obtained in these pharmacophore models was the presence of a hydrophobic interacting region along the alkyl chain and significance of furan moiety in ligand protein interaction as there is a decrease in inhibitory activity by 4-fold with reduction of furan moiety. Furthermore, it was observed that 8-Alkyloxyfuranocoumarin analogues inhibit CYP3A4 in a dose-dependent pattern and with average effectiveness [68].

**Table 2:** Overall table for pharmacophoric models of CYP3A4 inhibitors [67]

| Model No | Hydrophobic (HYD) | Hydrogen bond acceptor (HBA) | Hydrogen bond donor (HBD) |
|---|---|---|---|
| **1** | 3 | 1 | - |
| **2** | 3 | 2 | - |
| **3** | 1 | 3 | - |

Comparison of all the above studies reveal that the presence of one hydrophobic and one hydrogen bond acceptor features are necessary in the inhibitors of CYP3A4 enzyme. Disparity in the pharmacophoric models is observed in the above studies as diverse studies utilize different set of compounds with varying structural features.

### 2.2.2 QSAR models (2D, 3D and GRIND):

Various 2D and 3D QSAR models of different data series of CYP3A4 inhibitors and substrates have been constructed in the past few decades to understand the 3D structural features involved in CYP3A4 inhibition.

Riley *et al.* built a comprehensive quantitative physicochemical CYP3A4 inhibition model using diverse dataset of 30 inhibitors CYP3A4. The study revealed that the lipophilicity of compounds was important feature in the dataset of inhibitors. The presence of a pyridine, imidazole or triazole functional groups at terminal position increases the

effectiveness CYP3A4 inhibitors by approximately 10-fold for a given value of lipophilicity (LogD7.4) [69]. Another 2D QSAR model was built for a data set of 53 structurally diverse drugs. For each drug, a total of 220 two-dimensional topological indices were calculated. A through comparison between 3D QSAR models with 2D models reveals that the 2D QSAR disregard the uncertainties that are related to conformations and alignment in case of 3D QSAR. Moreover, the 2D descriptors are less extensive computationally and are completely automated. However, most restrictive feature of 2D-QSAR method is it does not considers the stereochemistry of the ligands under investigation and the information obtained from 2D-QSAR is lacking for further use in designing new drug molecules. In contrast, 3D-QSAR methodology provides graphical illustration of pharmacophores thus, aids in designating the optimum course for rational drug design. In vision of these proclamations it is concluded that both approaches are useful for screening of simulated compounds as they supplement one another depending upon the purposes of their application at different screening phases. However, both of the models showed insensitivity to the stereochemistry of training and test data sets.

A combination of genetic algorithm and partial least squares method (GA-PLS) was used in this study, which resulted in automatic selection of preferred descriptors and thus, maximizing the predictability of the $IC_{50}$ values. In previous studies the importance of hydrophobicity for CYP ligands has already been discussed and as hydrophobicity is reliant on the molecular volume, thus in this study the molecular size was considered to be an important descriptor for understanding ligand interactions with CYP 3A4. [36].

QSAR models of CYP3A4 enzyme inhibition were reported in this study. A total of four large data sets were used that comprises of marketed as well as drug-like compounds. All tested against four different substrates of CYP3A4 which were benzyloxycoumarin, testosterone, benzyloxyresorufin, and midazolam. First of all QSAR modeling method was

employed on one data sets which did not resulted in beneficial *in silico* predictive models for analysis of chemical libraries. Next MPH (multiple pharmacophore hypothesis) was formulated and tested. That resulted in improved QSAR models and also provides us with insight on ligand enzyme interaction. The idea of a multiple pharmacophore hypothesis delivered a distinctive concept for building QSAR models and understanding of inhibition of the metabolizing enzyme CYP3A4 [70].

Another QSAR model was developed by Roy *et al*, for studying the binding affinity as well as selectivity of CYP3A and CYP2B subfamilies ligands utilizing GFA (genetic function approximation) and G/PLS (genetic partial least squares) techniques. The studies were performed by utilizing electronic, spatial and topological as well as thermodynamic descriptors. The binding affinity models that were obtained had high statistical quality. The final model reveals the significance of topological, steric and electronic descriptors towards biological activity [71]. In another study both structure based as well as ligand based techniques were conducted using software Ligand Scout and Catalyst. Important structural features for substrate and inhibitors of five P450 enzymes P450 1A2, P450 2C9, P450 2C19, P450 2D6, and P450 3A4 were extracted. It was concluded that overall a CYP3A4 substrate based model reflect that there are three hydrophobic and two HBA features are involved in substrate and enzyme interaction demonstrating that hydrophobic interactions affinity as well as hydrogen bonding contribute in binding of substrate with enzyme. The inhibitors based model consists of two hydrogen bond acceptors (HBA) and four hydrophobic (HYD) features. Hydrophobic interactions are dominant in the reported CYP3A4 substrate and inhibitor based pharmacophoric models which was in agreement with the hydrophobic nature of the binding pocket of the enzyme already reported by Riley *et al*. [72].

In all these studies most important descriptors required for interaction of ligands with CYP3A4 that were identified were lipophilic, molecular sizes, topological, steric and electronic descriptors.

COMFA model have been developed by Ananthula, *et al*, using a dataset of phenyl ethanolamine class of compounds. The descriptors calculated were steric and electrostatic. CoMFA potential fields were calculated and contour maps were generated. The analysis of these contour maps proposed that the substitution of azetidin and oxadiazole rings at the position of acetaldehyde cause decrease in the inhibitory activity [73].

Shityakov and his coworkers developed CoMFA (Comparative Molecular Field Analysis) and COMSIA (comparative molecular similarity index analysis) models along with molecular docking methods using anthocyanin derivatives derivatives. The inhibitory activity of anthocyanin derivatives on enzyme CYP3A4 was studied in depth. CoMFA and CoMSIA models were built using 16 reported anthocyanin derivatives. These derivatives were obtained by the addition of hydroxyl groups at 3$^{rd}$ position of cyanidin ring or glycoside residues at 3$^{rd}$ and 5$^{th}$ positions. The most important interactions that were extracted after docking studies were π-π interactions involving amino acids Phe447 and Phe435. Additional interaction that contributed to the increased inhibitory effect of these derivatives significantly was hydrogen bond interaction involving amino acid Pro-434 interacting with OH group present in anthocyanin compounds[74].

The most important features obtained from above studies were steric and electrostatic. Major drawback of CoMFA and CoMSIA methodology was that the data of compounds on which they were performed should belong to congeneric series of compounds. The molecules should be superposed on one another. Hence, the procedure is time consuming. The consistency of the final model is also dependent on accurate alignment of the ligands in a three dimensional space [75]. So, nowadays in drug designing techniques GRIND models are

employed as they are alignment free, less time consuming and more reliable models as compared to CoMFA and CoMSIA models [76].

A generalized proteochemometric model has been developed for analyzing as well as predicting interactions between P450 enzymes and their inhibitors. The dataset that was used for building the model was obtained from various research groups therefore, it included diverse set of compounds. The combination of z-scale and GRIND-descriptors create a model that is robust. In this study a generalized GRIND model was built for inhibitors of a number of CYP enzymes and important probe distances that were observed included distance between two hydrogen bond donors that are O-O nodes that was 15.6-16.4 Å, DRY- DRY nodes were situated 4.0-8.0 Å apart, O-N1 nodes were separated by a distance of 16.0-16.8 Å these distances were found to be a cause of increase in the inhibitory activity of the ligands. While the compounds having a distance of 7.6-9.6 Å between hydrogen bond acceptor and shape based descriptor that are N1-TIP nodes respectively were found to be less potent inhibitors[35]. A 3D-pharmacophoric model for CYP3A4 was made using GRIND-based approach in which a diverse dataset of 331 CYP3A4 inhibitors was used. In this model MIF (Molecular Interaction Fields) were also used along with GRIND. A strong correlation was generated between 3D-QSAR model and the MIFs. The most important features that were extracted from this model include two hydrophobic areas and one hydrogen-bond acceptor [77].

The common features obtained from overall ligand based studies were presence of hydrophobic groups, hydrogen bond acceptors and shape based descriptors. The general CYP3A4 descriptors involved in CYP3A4-ligand interactions involved shape, connectivity, electronegativity, polarizability and hydrophobicity based descriptors which are similar to the findings of Yap and Chen [78]. Despite the efforts put forth in all these studies none of the investigations highlighted the structural features or interaction of stereoisomeric inhibitors

with CYP3A4. Thus, it is imperative to investigate important 3D structural features and ligand-protein interaction of stereoisomeric inhibitors with CYP3A4.

### 2.2.3 Classification Models:

A number of PLS models were built for studying the inhibition of CYP3A4-mediated erythromycin N-demethylation using different molecular descriptors [37]. The data set of 241 inhibitors and 368 substrates was used in SVM (support vector machine) classification method along with extensive cross-validation to categorize CYP3A4 inhibitors. Significant descriptors that were utilized in this study include electrostatic, hydrogen bond acceptors, hydrogen bond donors, hydrophobic, shape and size. It was observed that all SVM models performed well than the PLS discriminant analysis models [37, 79] .

A virtual screening sieve for classifying CYP3A4 library was established by using PLS regression along with ANN classifier. The PLS model with different molecular descriptors was able to correctly calculate and predict almost 95% of molecules in the training set (n = 311) and 90% of a semi-independent validation set of 50 compounds. This approach gave more accurate results as compared to ANN (artificial neural network) approach applied on the same dataset. PLS prediction model is now employed on regularly in our virtual screening cascade [80].

In all the above ligand based and structure based studies the stereo-selectivity of the inhibitors was not discussed in detail and either single enantiomer or recemates of the drugs were used. Therefore, in the present study 2D and 3D features of the enantiomeric pairs of CYP3A4 inhibitors are investigated. Their docking studies are conducted to extract important interactions between CYP3A4 enzymes and the inhibitors.

***Chapter 3***

# Methodology

Combined structure and ligand based methods were used to identify differences in distances of important pharmacophoric features of the enantiomeric pairs of CYP3A4 inhibitors. Overall, work flow of the methodology is shown in the figure 6.

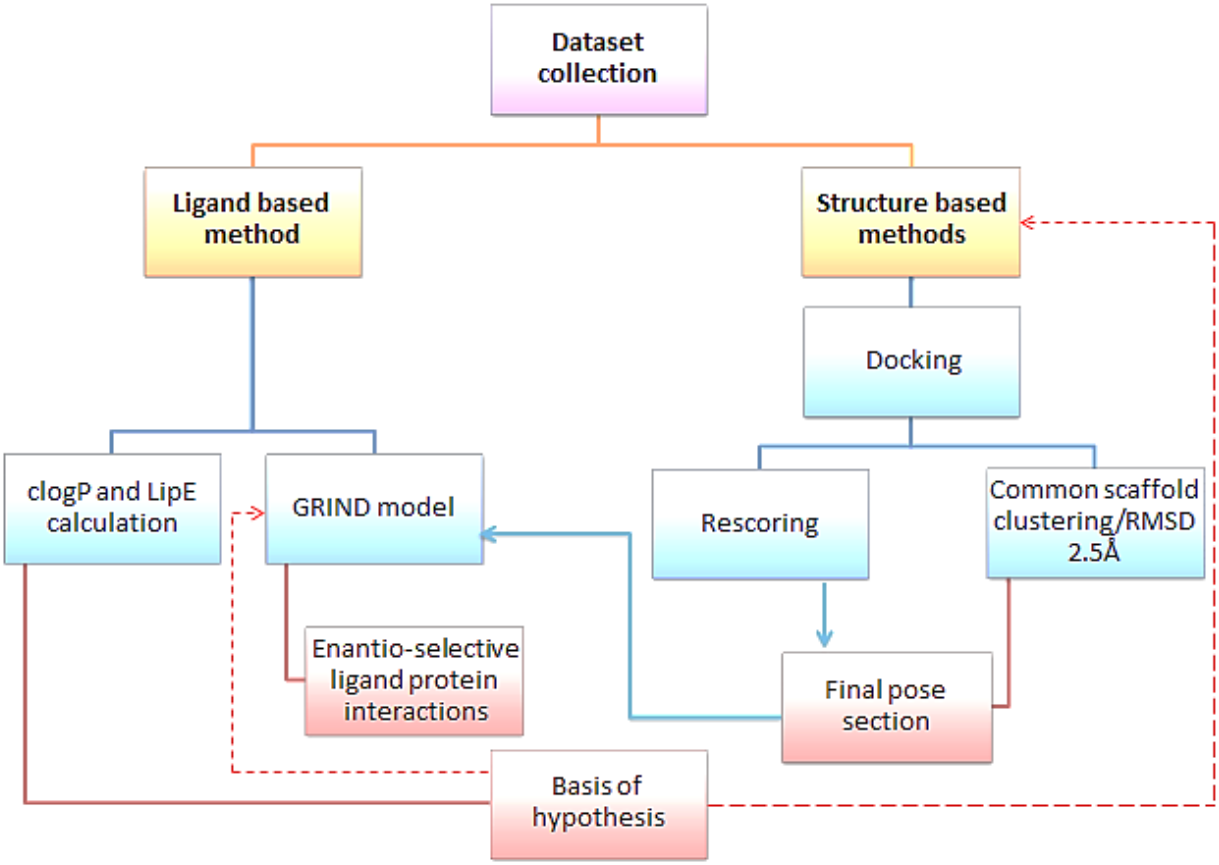


**Figure 6**: Overall work flow of the methodology used in the present investigation

## 3.1. Database:

A series of CYP3A4 inhibitors were extracted from literature. A total of 9 inhibitors were selected having both R and S stereoisomers. Stereoisomers showed significantly different inhibitory values ($IC_{50}$), while the ligands which doesn't showed significant difference in the values of $IC_{50}$ e.g. ketamine R and S isomers were also included in the data

set along with those compounds which showed significant difference in $IC_{50}$ values for example verapamil R and S isomers. So that comparison can be done that how different stereo-inhibitors of having varying inhibitory potencies interact with CYP3A4 enzyme. Moreover, in vitro inhibitory concentrations ($IC_{50}$) of the molecules having both S and R forms along with their $IC_{50}$ values against CYP450 3A4 were only added in the dataset.

All these ligands were extracted from studies which reported $IC_{50}$ values for both S and R isomeric forms of same inhibitor. The SMILES structures of the compounds were constructed using Chem-Draw Pro 8.0 software, while keeping in consideration the stereoisomeric forms or spatial orientation of atoms. Final 3D structures were constructed using these SMILES in Molecular Operating Environment (MOE) 2013.08 software [81].

**Norflouxetine**

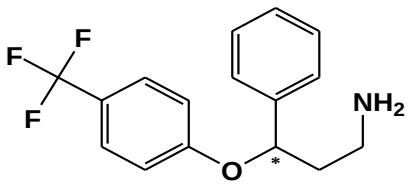


| Stereoisomers | $IC_{50}$ (µM) |
|---|---|
| R : | 5 |
| S : | 11 |

**Flouxetine**

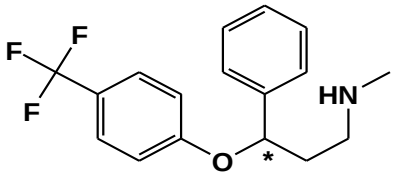


| Stereoisomers | $IC_{50}$ (µM) |
|---|---|
| R : | 80.00 |
| S : | 47.00 |

**Ketoconazole**

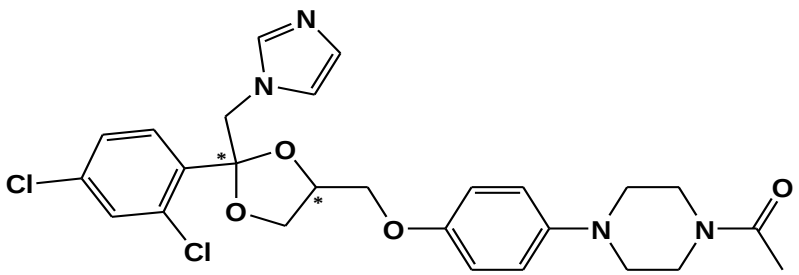


| Stereoisomers | $IC_{50}$ (µM) |
|---|---|
| 2S,4R : | 0.54 |
| 2R,4S : | 0.23 |

**Itraconazole**

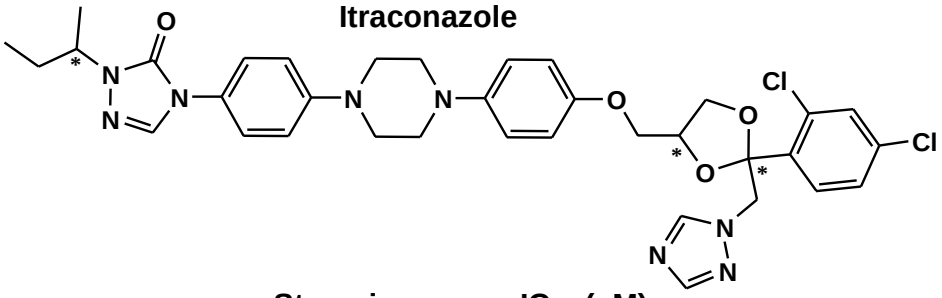

| Stereoisomers | $IC_{50}$ (μM) |
|---|---|
| 2R,4S,2R : | 0.0400 |
| 2R,4S,2S : | 0.0037 |
| 2S,4R,2R : | 0.0148 |
| 2S,4R,2S : | 0.0083 |

**Verapamil**

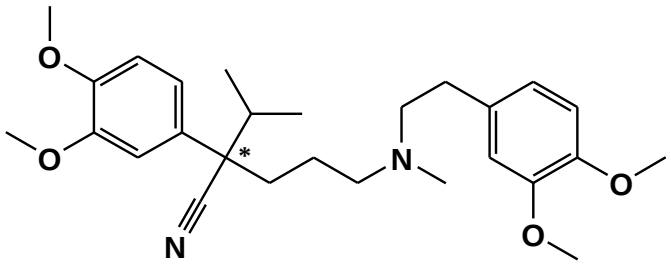

| Stereoisomers | $IC_{50}$ (μM) |
|---|---|
| R : | 6.460 |
| S : | 2.970 |

**Reboxetine**

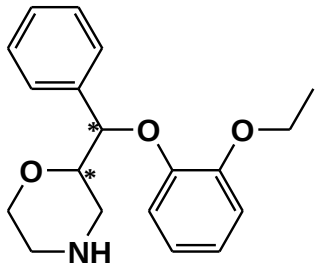

| Stereoisomers | $IC_{50}$ (μM) |
|---|---|
| R, R: | 14.300 |
| S, S: | 21.300 |

**Dichlobutrazol**

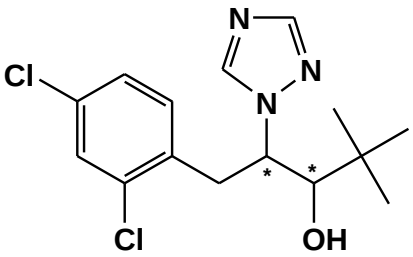

| Stereoisomers | $IC_{50}$ (μM) |
|---|---|
| R,R : | 0.75 |
| S,S : | 1.50 |

**Ketamine**

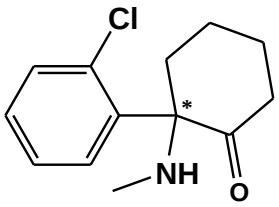

| Stereoisomers | $IC_{50}$ (μM) |
|---|---|
| R : | 0.27 |
| S : | 0.25 |

**Figure 7**: Stereoisomeric inhibitors of CYP3A4 and their $IC_{50}$ values taken from [82-88]

## 3.2. Lipophilicity (clogP) and ligand efficiency (LipE) calculation:

Lipophilicity (clogP) of a compound is associated with its binding in the active site and its rate of metabolism. Therefore, clogP was calculated for all the ligands and graph was

plotted between $pIC_{50}$ and clogP [89]. The graph displayed that although molecular weight and other phyisico-chemical properties like cLogP of stereoisomeric pairs are similar but their $pIC_{50}$ values are different from one another. Therefore, it leads to the investigation that either the difference in $IC_{50}$ values is due to difference in interaction between CYP3A4 and ligands or due to other pharmacokinetic parameters like absorption or distribution.

Lipophilic efficiency (LipE) is a parameter that is employed in drug design to assess the transport of compounds. Therefore, LipE of all the compounds in the dataset was calculated to understand the reason behind difference in $pIC_{50}$ values of stereoisomers of same ligand. Lipophilic efficiency links potency and lipophilicity in an endeavor to evaluate the drug-likeness of a compound [90]. For a given compound or ligand LipE is defined as the $pIC_{50}$ (or pEC50) minus the clogP of that compound. Equation is as follow[91]

$$LipE = pIC_{50} - clogP$$

### 3.3. Docking and Pose Analysis:

Docking was performed to analyze the difference in ligand-protein interaction pattern of stereoisomeric inhibitors in CYP3A4 active site and to obtain most native binding conformations of each ligand for further GRIND analysis. A dataset of 18 molecules were selected and docked in CYP3A4 enzyme. The crystal structure that was used for docking was 1TQN as it has best resolution of 2.05**Å** and very few amino acids were missing in this structure. Docking simulations were performed by employing the software GOLD suite v 5.3 [92]. The ligands were considered flexible but they were not allowed to alter the stereo-conformations around the chiral centers. Binding site was selected by analyzing the orthogonal x, y and z coordinates around the centroid point that is single-solvent accessible point which is present approximately in the center of the active site. The radius was set to 13**Å** that was approximate radius of the active site including all important amino acid residues. A sum of 100 genetic runs for every ligand was executed. Scoring function GOLD

score was used for ranking the resulting poses for each ligand. Slow protocol was used as it is the most accurate protocol.

Best scoring poses were obtained by using both methods of rescoring/consensus scoring and common scaffold clustering. 1800 poses for 18 ligands were generated which were further rescored using ASE, affinity DG, alpha HB and London DG scoring functions. Best scored poses were further nominated for investigating ligand protein interactions. Additionally to supplement the results from rescoring common scaffold clustering was performed for two sets antidepressants and antifungals both consisting of 600 conformations for a total of 6 ligands three pairs for each class. Clusters were obtained on the basis of RMSD and best cluster and conformations were selected on the basis of rescoring. The cluster III was selected for antidepressants as it consisted of best scored conformations. Best rescored conformations were selected in case of antifungals as both clusters present in 2.5Å RMSD group bound at same binding position in CYP3A4 enzyme. Moreover, to circumvent errors in selection of final conformation, the final selected conformations were accredited with previously existing mutagenesis and structural activity relationship data. Best conformations of these 18 ligands were further employed in GRIND analysis.

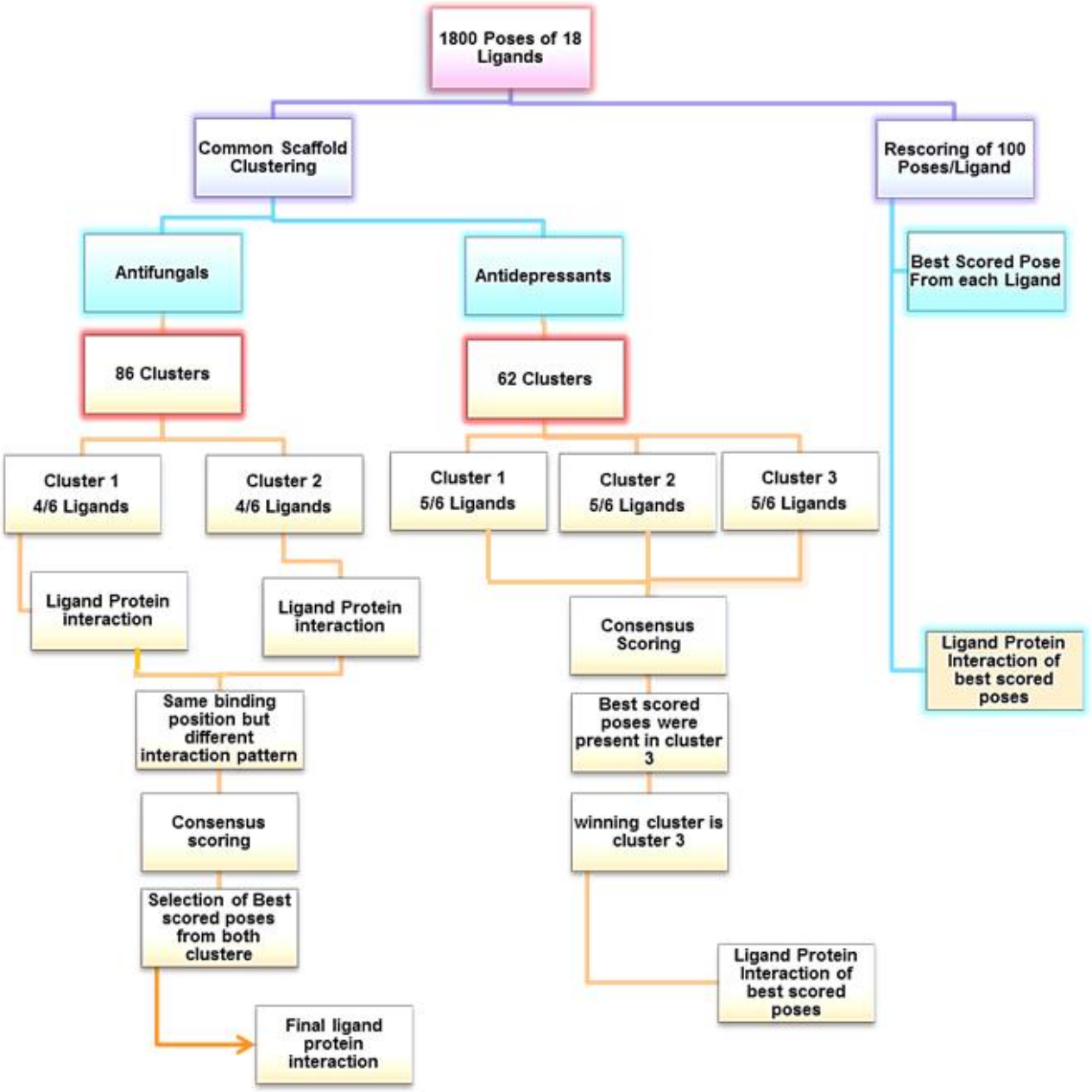


**Figure 8**: Work flow for selection of final conformations

### 3.4. GRIND Models:

Three dimensional conformations of ligands were generated in Molecular Operating Environment (MOE) 2013.08 software using SMILES obtained from ChemDraw. These structures along with their biological activities were imported in Pentacle version 1.05 (March 2010). Molecular Interaction Fields (MIFs) were calculated by employing four different probes that are:

1. ‘DRY’ representing hydrophobic interactions,
2. ‘O’ sp2 carbonyl oxygen represents Hydrogen bond donor,
3. ‘N1’ is Hydrogen bond acceptor
4. ‘TIP’ explaining molecular edges.

All the probes are placed at every node on the grid and molecule-probe energy of interaction is computed [93]. Total energy at each node is calculated by using the following equation:

$$E_{xyz} = \Sigma E_{lj} + \Sigma E_{el} + \Sigma E_{hb}$$

Where $E_{lj}$ is Lennard-Jones energy, $E_{el}$ is electrostatic energy and $E_{hb}$ is hydrogen bond energies at that point. Furthermore most important and relevant MIFs are to be mined that was done by using algorithm AMANDA provided in the package [94]. Consistently large auto and cross correlation (CLACC) algorithm was used for encoding the final nodes into GRIND thus producing consistent sets of variables. As CLACC orient the compounds according to their moment of inertia and thus it roughly aligns important pharmacophoric features of the ligands so consistent nodes are selected. The values attained from encoding were directly represented in correlogram plot. The QSAR model was built using PLS. Models with statistically significant $q^2$ and standard error values were further analyzed.

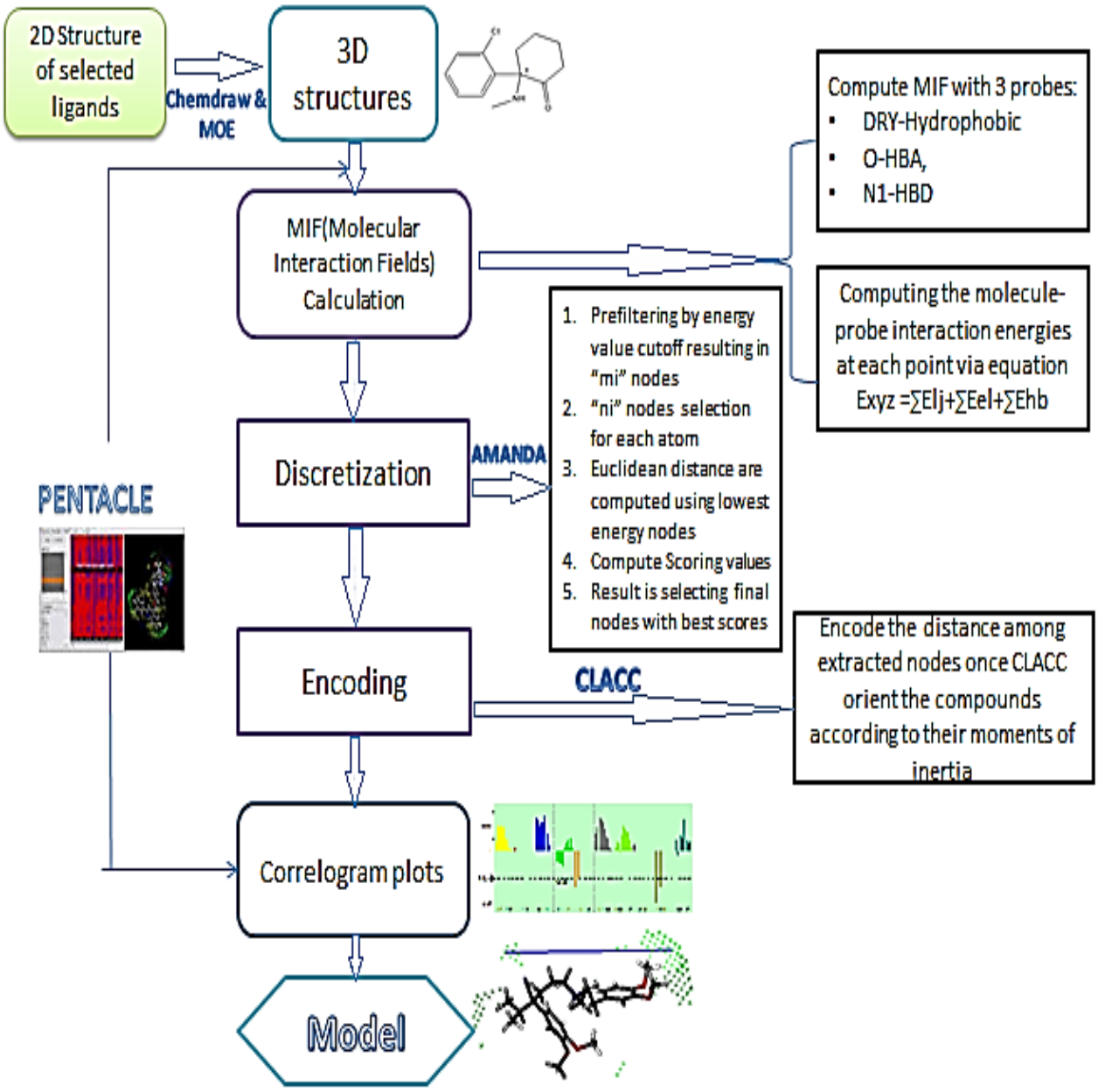


**Figure 9**: Work flow for building GRIND model

***Chapter 4***

# Results and Discussion

## 4.1. Stereoselectivity in CYP3A4 inhibition:

Inhibitory activities in the collected dataset were varying among the stereoisomeric pairs of the inhibitor. The difference between the $IC_{50}$ values ranged from very less for e.g. in ketamine that is less than 1 order of magnitude (R/S: 0.27/0.25µM) to significant difference for e.g. in verapamil the $IC_{50}$ value differ between R and S enantiomers by 2 orders of magnitude (R/S: 6.46/2.97µM). Similarly, in enantiomers of Dichlobutrazol the difference of $IC_{50}$ values is by 1 order of magnitude (R/S: 0.75/1.5µM). Inhibition studies already performed on enantiomers have shown the significance of analyzing stereoisomeric compounds and stereochemistry. Generally, studies illustrate that one enantiomer can show higher inhibitory or activity potencies as compared to its counterpart isomer[83] .

Although these isomers have same structure and there general physico-chemical properties are similar but they differ from one another due to spatial orientation of four different groups around the chiral center. Even though the difference between activities of various stereoisomeric drugs has been discussed however, it remains to be analyzed the vital cause of that difference. Either it is due to difference in the interaction of drug with the target or due to the way of the drug to the target target/different ADME properties. This query is the basis for calculating lipophilicity (clogP) and lipophillic efficiency (lipE).

## 4.2. Lipophilic Efficiency (LipE) and Lipophilicity (clogP) calculation and significance:

Lipophilicity (clogP) was calculated using chemdraw software and graph was plotted between $pIC_{50}$ on y-axis and clogP on x-axis as shown in figure 10. The lipophilicity of drugs is important as the physiologiocal environment of human body is lipophilic in nature.

However, in order to cross various lipophilic barriers within the body a drug molecule have to maintain a balance between lipophillicity and hydrophilicity. Various studies indicate a direct correlation between lipophillicity and inhibitory potency of the drugs e.g. clotrimazole and miconazole have clogP values 5.25 and 5.81 respectively are both strong inhibitors of CYP3A4 [95, 96]. In the present dataset the clogP values for some ligands were in the range of 2.23 to 7.13. Itraconazole was highly liphophilic with a clogP of 7.13. Though all the stereoisomers of Itraconazole have same clogP value of 7.13 but their activity values ($pIC_{50}$) were different ranging from 7.397 to 8.431. Similarly, in case of dichlobutrazol and fluoxetine the clogP value was almost similar that is 4.26 for dichlobutrazol and 4.27 for both isomers of fluoxetine but the difference in $pIC_{50}$ values is significant ranging from 4.096 to 6.124 as shown in figure 10. This was the basis of hypothesis to further investigate the reason for difference between $IC_{50}$ values of different enantiomers of same ligand.

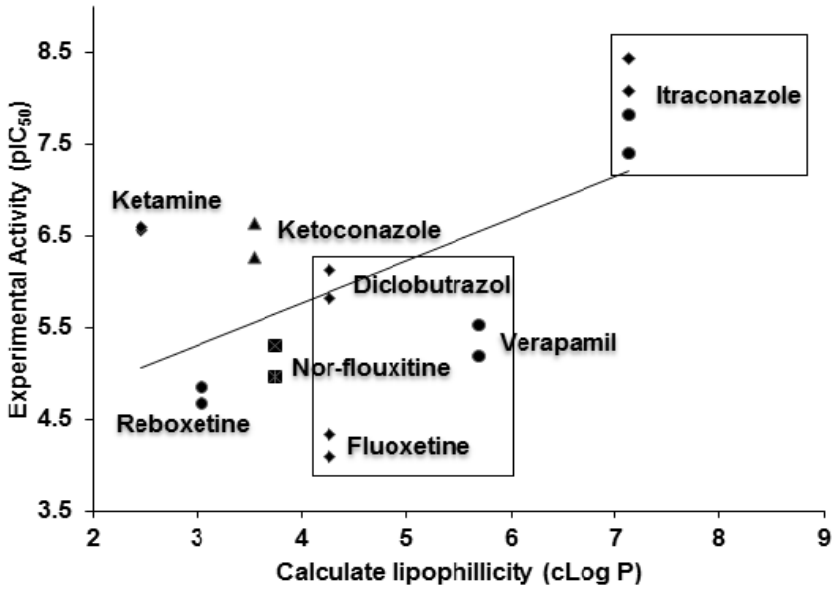


**Figure 10:** Graph between $pIC_{50}$ of inhibitors of cyP3A4 and their cLogP values

Lipophilic efficiency was calculated further to predict that how efficiently the drug reaches its target inside the human body. As shown in the following graph that all the stereoisomers of same drugs have almost similar lipE values. Both the stereoisomeric pair of itraconazole has almost same lipE values. Out of the four stereoisomers three isomers that are

2R,4S,2R 2S,4R,2R and 2S,4R,2S have lipE value above zero and fourth isomer 2R,4S,2S value above 1. In remaining dataset rest the enantiomeric pairs have approximately same lipE values as shown in figure 11..

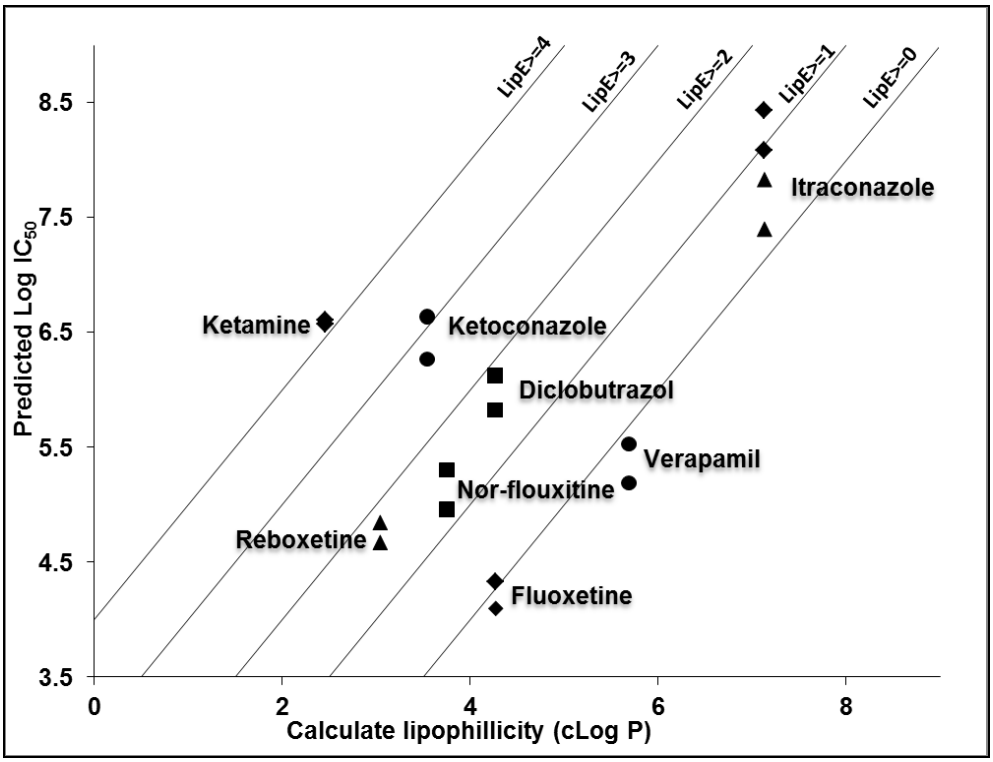


**Figure 11:** Graph between $pIC_{50}$ on y-axis and cLogP on x-axis along with LipE values.

As a result it can be hypothesized that the difference in the activities among the stereoisomers is not due to lipophilicity/pharmacokinetic pharmacokinetic parameters of the drugs. Consequently we move towards the study of ligand protein interaction of these stereoisomers with CYP3A4 enzyme.

## 4.3. Docking:

### 4.3.1. Protein structure selection:

Around 18 crystal structures of human cytochrome P450 3A4 have been published and are available on enzyme CYP3A4. Protein Data Bank has crystal structures of human CYP3A4 in both non-ligands bounded and ligand bounded form. 1TQN was selected that is non-ligand bonded while 3NXU and 4K9W are present in ligand bounded forms. 1TQN was

superposed on 3NXU and 4K9W as shown in figure 12. Carbon alpha chain RMSD (root mean square deviation) was calculated that was 1.795Å and 1.790Å for 3NXU and 4K9W respectively. When all three structures were superposed RMSD was 1.58Å. As overall the difference between these structures was not significant. However, the position of Arg212 is altered in case of ligand bounded and non-ligand bounded enzyme. As, in case of 1TQN the residue Arg212 is positioned closer to the heme inside the active site while in case of ligand bounded crystal structures 3NXU and 4K9W this residue is located away from the heme on the outer surface of the active site as shown in figure 12(B). Therefore, 1TQN was selected on the basis of high resolution that is 2.05Å and on the basis of its apostate [97].

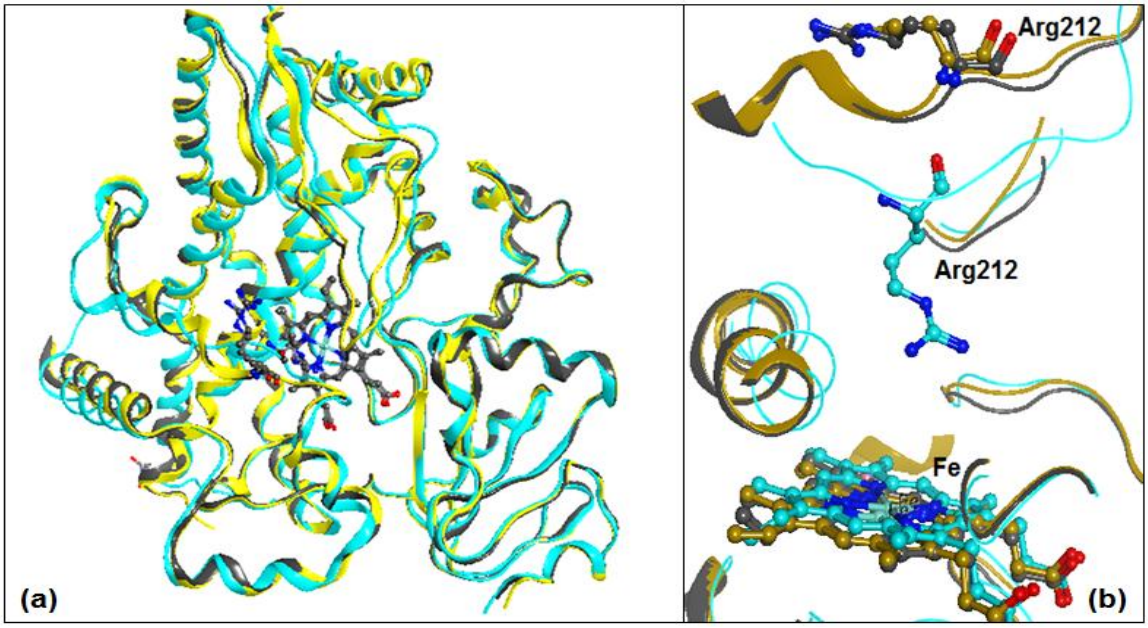


**Figure 12:** (a) Three superposed structures of CYP3A4 in which 3NXU, 4K9W and 1TQN are shown in gray, yellow and cyan color respectively, (b) position of arginine is shown in the figure in both ligands bounded and non-ligand CYP3A4 structures in case of 1TQN the Arg212 is closer to heme.

### 4.3.2. Pose generation and binding cavity:

Dataset of ligands previously discussed in methodology were used for docking in CYP3A4 enzyme. Binding cavity was selected on the basis of previous mutagenesis and docking studies as discussed in literature review. The most significant features of CYP3A4 binding cavity were its size, shape and promiscuous nature. The binding cavity size increase

as we move closer to between heme-iron of the enzyme. The two volumes of active site available in the literature are 520Å and 1386Å [44, 45]. Ligands of diverse size can be accommodated in the bind cavity due to its large size and therefore, more than one substrate can be accommodated inside the active site simultaneously. The active site was identified in GOLD suite v 5.3 by using centroid atom and adjusting its x, y and z coordinates. The x, y and z were -19.6730, -20.0160 and -9.8128 respectively and the cavity range was 13Å. In GOLD suite software genetic algorithm was used to generate multiple poses for each ligand. In this study 100 poses were generated for each ligand to certify reproducibility and precision of the employed protocol and scoring function gold score was used.

### 4.3.3. Pose evaluation:

Two methods were employed for pose selection

- Consensus scoring
- Common scaffold clustering.

#### 4.3.3.1. Consensus scoring:

All the poses were rescored using ASE, Affinity dg, Alpha hb and London dg scoring functions in MOE 2013.08 software. 18 best ranked poses were selected for each ligand out of 1800 ligands that were further used for final ligand protein interaction. Each ligand protein interaction was studied and it was observed that pi-pi interaction with Phe-215 was common among all the ligands.

Other interactions that were observed include hydrogen bonding and electrostatic interaction, involving amino acids residues Glu-374, Phe-213 and Ser-119 etc. The stereisomer that is more active as compared to its counterpart isomer showed better fitting in the active site as was observed in case of verapamil and itraconazole as is shown in figure 13 and 17 respectively. Except for those pairs in which the difference between the activities of

isomeric pair was not significant showed similar type of ligand protein interactions for e.g. ketamine as shown in the figure 13(a). Those in which the difference was significant for e.g. in case of verapamil its S form showed stronger hydrophobic interaction inside the binding pocket with Phe-108, Phe-215, Phe-57 and Tyr-53 as compared to R verapamil as shown in figure 13(b). All the winning poses were interacting with amino acids that are already known to be involved in interaction by structure based and mutagenesis studies as shown in figure 14.

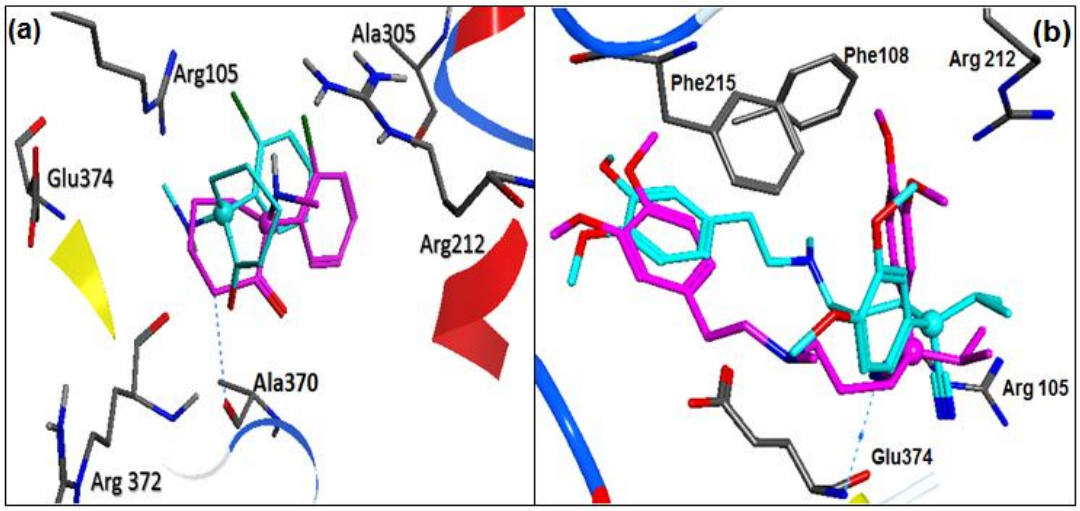


**Figure 13:** Presentation of docked complex for CYP3A4 with: (a) ketamine, (b) verapamil, CYP3A4 interaction residues and both R and S isomers of ligands are shown in the figure where cyan color is for R isomer while magenta color is for S isomeric forms, while balls represent the chiral centers.

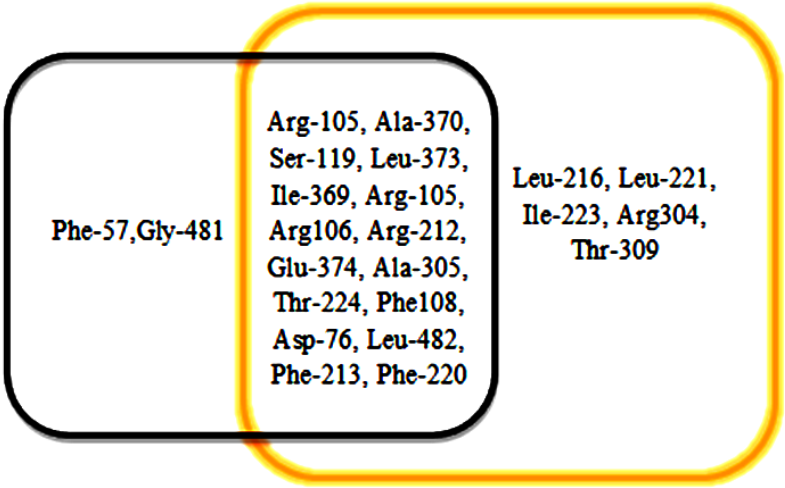


**Figure 14:** Overlapping important amino acids in the literature review (orange box) compared with present study (black box) are shown **[57, 98, 99].**

#### 4.3.3.2. Hierarchical Cluster Analysis:

Common scaffold clustering was done on two sets of ligands containing common scaffold, it includes three pairs of stereoisomers of antifungals and antidepressants. Common scaffold of both classes is shown in figure 15.

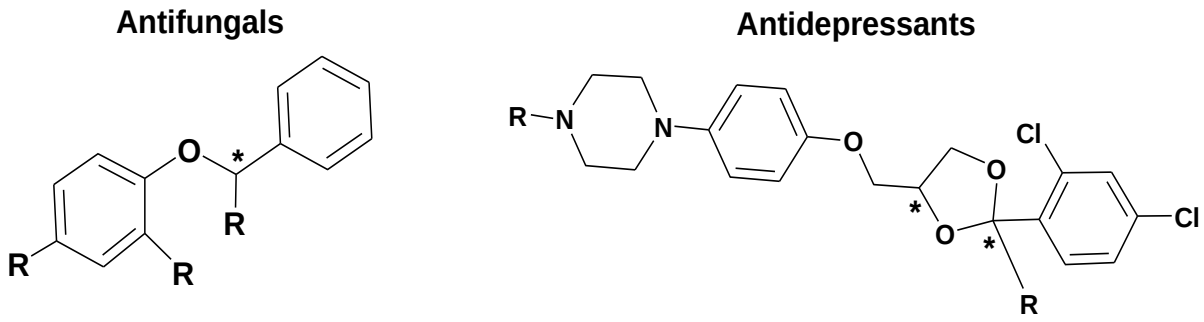


**Figure 15:** Common scaffold of antifungals and antidepressants used in Hierarchical cluster analysis where steric represent the chiral centers.

In case of antifungals a total of 86 clusters were obtained at 2.5Å RMSD. Two clusters consist of 4 out of 6 docked ligands. Binding position inside the active site of both clusters was analyzed for final cluster selection. Both clusters showed same binding position and interacting amino acids. The interacting amino acid residues involved were Ile-369, Arg-372, Phe-215 Phe-220, Arg-212, Ala-305 and Glu-374. Consensus scoring was done and those poses from both the clusters as I and II were selected on the basis of best ranks. Final poses have been selected for further ligand protein interactions analysis. It was observed that the 2R,4S,2S and 2S,4R,2S stereoisomers of itraconazole having low $IC_{50}$ value of 0.0037µM and 0.0083µM respectively showed better interaction in the binding cavity as both these isomers showed stronger electrostatic interactions with Ala-370 and Gly-481 as compared to 2R,4S,2R and 2S,4R,2R isomers of itraconazole. The results were compared with available literature and it was observed that same amino acid residues namely Arg105, Arg-106, Arg-212, Ile-369, Ala-370, Glu-374 and Arg-372 that were involved in interaction were also identified to be present in previous studies performed on six flavone inhibitors of CYP3A4 [60].

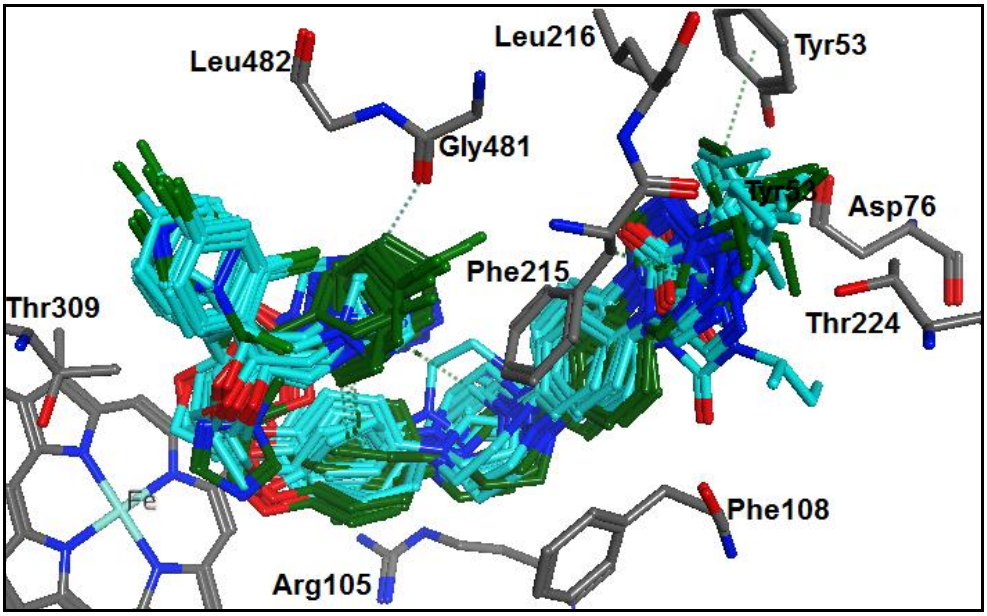


**Figure 16:** Cluster no I and II are shown in the green color and cyan color respectively.

In second set common scaffold clustering was done on poses of three pairs of stereoisomers of antidepressants namely fluoxetine, nor-fluoxetine and reboxetine. Total 62 clusters were obtained at 2.5Å RMSD. Out of 62 three clusters namely I, II and III consisted of 5 out of 6 docked ligands at 2.5 RMSD. All three clusters I, II and III showed varying binding positions inside the active site as shown in figure 17. However, none of the cluster showed significant difference in the interacting amino acids residues including Phe-108, Phe-215, Arg-212, Arg-105, Leu-373 and Ala-305 that were involved in ligand protein interactions. Therefore, to select final cluster consensus scoring was done and cluster no III was selected as this cluster consisted of maximum number of best ranked poses.

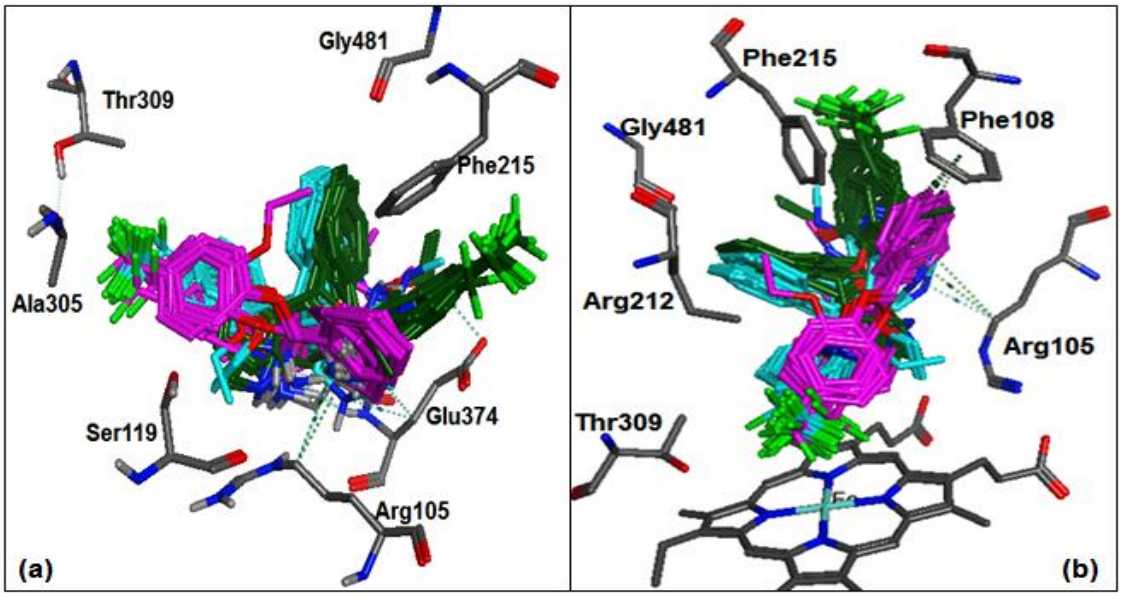


**Figure 17:** All the three **I, II and III** overlapped clusters are shown in the figure in cyan, magenta and green colors respectively (a) in this figure all three clusters are presented horizontally (b) In figure b all three clusters are presented vertically and heme is also shown.

#### 4.3.3.3. Final poses selection:

Final pose selection was based on the investigation that which of the conformations either from consensus scoring or from common scaffold clusters was discriminating more clearly between the stereoisomeric pair and their interactions with the enzyme. Conformations obtained from common scaffold clustering were selected for further GRIND analysis as they were differentiating between R and S isomers more evidently. The ligands that were not analyzed using common scaffold clustering were taken from consensus scoring.

Ligand protein interaction of all the winning conformations in the dataset were analyzed out of which fluoxetine, reboxetine and both pairs of itraconazole revealed significant difference in the interaction pattern of isomeric pairs as shown in figure 18. Similarly, in case of nor-fluoxetine and dichlobutrazol the interaction pattern of more potent isomeric forms were significant and differentiating while in case of ketamine the both pairs of enantiomers showed almost similar interaction pattern as shown in figure 13(a), which further strengthen the less difference in the $IC_{50}$ values of R and S isomers of ketamine that is 0.27

and 0.25 respectively. In case of nor-fluoxetine (R/S: 5/11µM) its R isomer is showing stronger interactions in the active site with Glu-374, Arg-105 and Arg-372 and its ether oxygen is also involved in interaction as compared to its S isomer. Similarly in case of dichlobutrazol (R/S: 0.75/1.5µM) its R isomer shows stronger hydrogen bonding interactions with Arg-105 and Ala-370 while its S isomer is showing water mediated hydrogen bonding interaction with Ser-119. It was identified that S-fluoxetine show better fitting inside the binding pocket as compared to R fluoxetine. As, the ether oxygen in S-fluoxetine and its secondary nitrogen group show stronger hydrogen bonding interactions with Glu-374, heme and Arg-105 as compared to R-fluoxetine as shown in figure 18(A). Similarly, in case of reboxetine R-isomer showed stronger hydrogen bonding interactions as compared to its S-isomer inside the binding pocket with Ala-370 and Glu-374 which is due to different orientation of groups around the chiral center. It also showed additional hydrophobic interaction with Phe-57 as shown in figure 18(B). 2S, 4R, 2S-itraconazole showed better electrostatic interaction with Ala-370, Gly-481 and hydrogen bonding with Arg-372 as compared to 2S, 4R, 2R-itraconazole as shown in figure 18(C). All these amino acids including Ala-370, Glu-374, Arg-105, Arg-372 and Ser-119 are important in interaction of ligands with CYP3A4 enzyme as discussed in a study by Hayes, *et al,* in which GOLD dock was used to study ligand protein interaction of about 195 ligands with CYP3A4 to elucidate promiscuous nature of this enzyme [100].

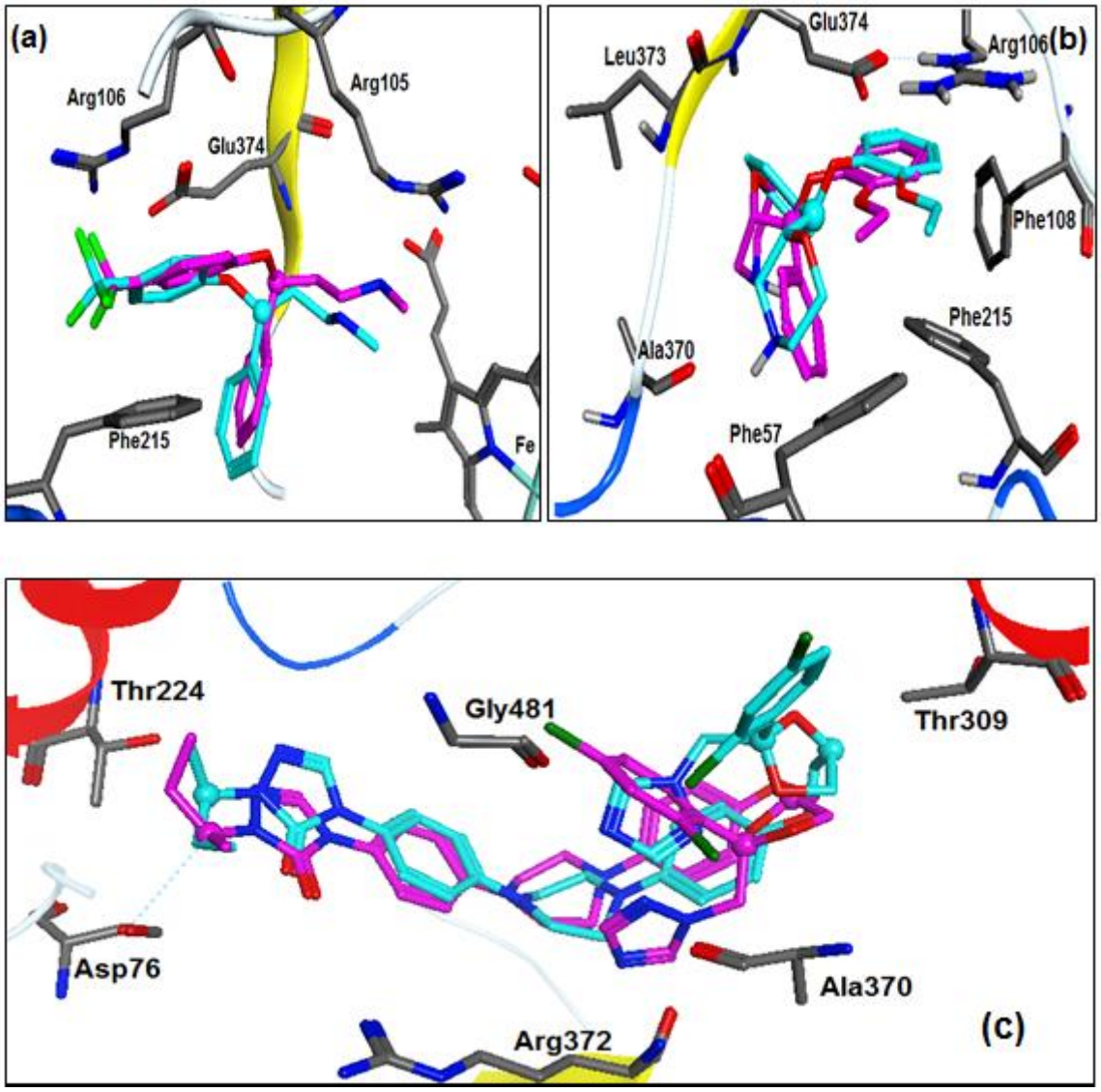


**Figure 18:** Illustration of docked complex for CYP3A4 with: (a) fluoxetine, (b) reboxetine , (c) itraconazole, CYP3A4 interaction residues and both R and S isomers of ligands are shown in the figure where cyan color is for R isomers while magenta color is for S isomeric forms. The dotted lines denote hydrogen bonding and balls represent the chiral centers.

## 4.4. GRIND analysis:

In order to correlate the difference in biological activity of different stereoisomeric pairs with discrete difference in the distance matrices of 3D structural features at stereocenters, GRID independent molecular descriptor analysis of the final binding conformations of all stereoisomeric pairs in the data set have been carried out using software Pentacle v 1.06.[101]. The molecules and their biological activities ($pIC_{50}$) were loaded in the software. Molecular descriptors were computed and discretized using AMANDA algorithm

implemented in Pentacle software. Finally encoding was done using CLACC algorithm and correlogram were generated.

PLS (partial least square) model was built using 5 latent variables. Initially complete set of variables was used to build the model but the result was inadequate as shown in table. Afterwards when one cycle of FFD variable selections was applied, the model showed improvement in statistics (shown in table 3).

### 4.4.1. Model statistics:

In the following table 3 $Q^2$ and $R^2$ are given for both complete set of variables and after one cycle of FFD, in which non-consistent variable are excluded from the model.

**Table 3:** Statistics of preliminary GRIND models using complete set of active variables

| | **$R^2$** | **$Q^2$** | **FFD** | **SEP** |
|---|---|---|---|---|
| **Complete set of variables** | 0.71 | 0.60 | 552 | 0.80 |
| **One FFD cycle** | 0.77 | 0.69 | 430 | 0.70 |

### 4.4.2. Graph between actual and predicted $IC_{50}$ values:

Model that was obtained after one cycle of FFD having $R^2$=0.77 and $Q^2$ =0.69. This model was further validated using LOO (leave one out) cross validation. With the exception of ketamine which was under predicted and its residual value was greater than one log unit (R/S; $IC_{50}$: Actual/Predicted, 0.56: -0.92/0.602: -0.87) as shown in the figure 19 in which ketamine is shown in the shape of triangles. This difference in actual and predicted biological activity of ketamine is might be due to the fact that all the compounds in the dataset are hydrophobic in nature having clogP values ranging from 3.04 to 7.13, while ketamine consisted of lowest clogP value that is 2.46. However, the important descriptors that emerged in the present GRIND model are hydrophobic in nature. As it is analyzed in previous studies that lipophillicity of compounds play an important role in the interaction of ligands with

CYP3A4 so ketamine having low lipophillicity showed different behavior and act as an outlier in the dataset [102].

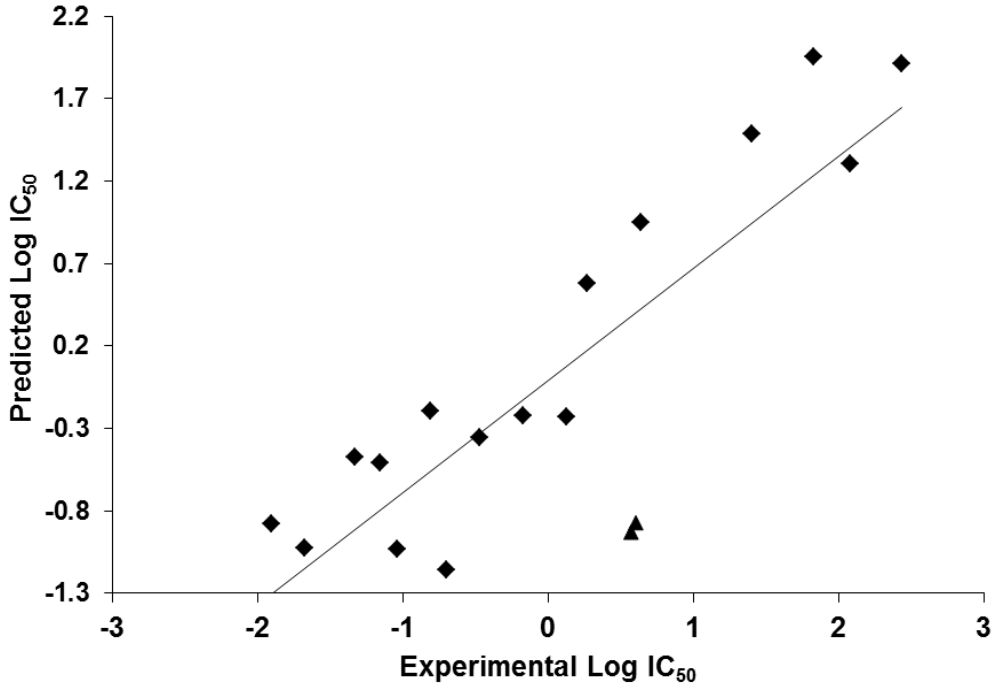


**Figure 19:** Internal validations of CYP3A4 inhibitors model based on docking conformations using leave one out cross validation method

### 4.4.3. Correlogram:

PLS co-efficient plot of GRIND model was used to analyze and identify features that play an important role in interaction of inhibitors with CYP3A4 enzyme. The bar plot shown in figure 20, demonstrate that DRY-DRY and DRY-TIP are important features that show positive contribution in the inhibitory activity of ligands while O-TIP and O-O contribute negatively towards the activity of CYP3A4 inhibitors.

Furthermore, investigation of the correlograms reveals that the features N1–N1, DRY–N1 and N1–TIP contribute positively in the inhibitory activity of the ligand and also differentiate between the stereoisomeric inhibitors of itraconazole and

ketoconazole.

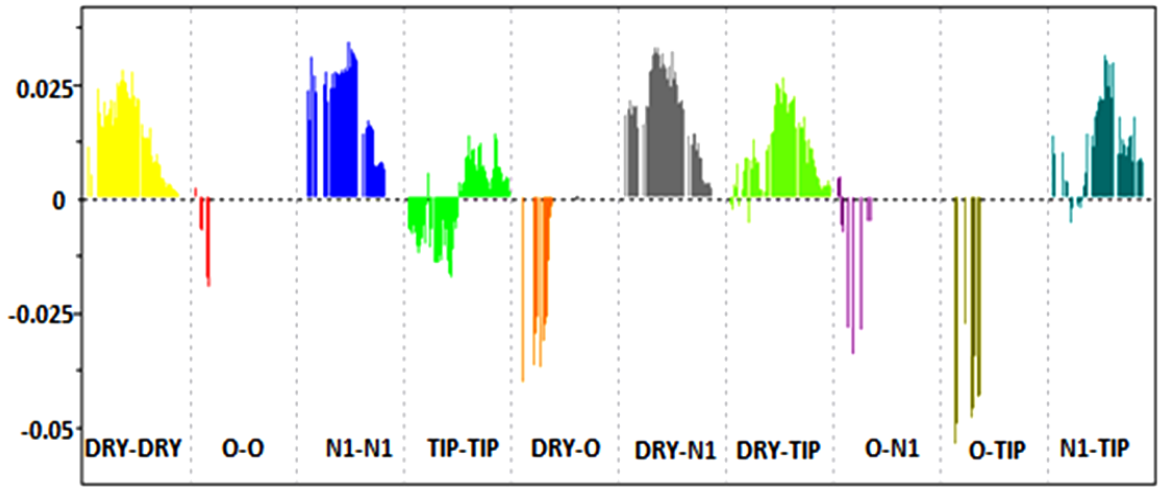


**Figure 20:** PLS co-efficient profile of positively and negatively correlated variables of stereoselective CYP3A4 inhibitors

Docking studies of stereoisomeric CYP3A4 inhibitors also revealed that the presence of hydrophobic and bulky groups in the ligands results in better fitting of the ligands in the binding pocket. The presence of hydrophobic regions increases the inhibitory potencies of the ligands is also established in previous studies of CYP3A4 inhibitors. In a study by de Groot, *et al*, three hydrophobic and two hydrogen bond acceptors were identified to be important pharmacophoric feature in the inhibitors of CYP3A4 [103]. Similarly, in a study by Didziapetris, *et al*, who predicted in his work that when the size of a ligand is increased by incorporation of a hydrophobic or an aromatic residue it results in a higher probability for the ligand to inhibit CYP3A4 [104].

DRY-DRY set of variables in PLS co-efficient correlogram (figure 20) shows that optimal distance of about 12-12.4Å between two hydrophobic regions contribute positively in biological activity of CYP3A4 inhibitors. This distances separate R and S isomers of itraconazole and ketoconazole as two hydrophobic features are more pronounce in S isomer as compared to R isomeric form. This feature characterize the distance between the two triazol rings in case of itraconazole S isomers while in case of R isomer is the distance calculated between benzene and triazol ring. Similarly, in case of S-ketoconazole the DRY-

DRY distance is between central benzene ring and a terminal dichlro-phenyl ring present in the structure as shown in figure 22(a). It is also evident from previous studies that hydrophobic features are important in the interaction of ligands with CYP3A4 [103]. Similar results were also observed in a study conducted on CYP3A4 inhibitors in which the DRY-DRY distance observed was approximately 11.5 **Å** [77]**.**

Previous studies have also discussed the importance of hydrogen bond acceptor in CYP3A4 inhibitors for example in a pharmacophoric based study by Schuster in 2006 it was identified that the presence of four hydrophobic and two hydrogen bond acceptors are necessary for interaction of inhibitors with CYP3A4 enzyme [72]. Similarly, in a detailed GRIND based analysis that was conducted on diverse dataset of 331 CYP3A4 inhibitors. Important descriptors and their distances that were extracted included DRY-TIP distance that is 16.5Å TIP-TIP nodes distance 20.5Å and DRY-DRY distance 11.5Å. A distance of about 12.5Å and 19.5Å of Hydrogen bond acceptor node from DRY and TIP nodes respectively was also stated to be significant for inhibition of CYP3A4 enzymes [77]. However, current GRIND model depicts two hydrogen bond acceptors at a distance of 16.8-17.2Å are important positive contributors in inhibitory potency of CYP3A4 inhibitors [77]. This feature is also a differentiating between R and S stereoisomers of itraconazole and ketoconazole. The distance between N1-N1 is observed among two triazol rings present in 2R, 4S, 2S isomeric form of itraconzole, while in case of 2R, 4S, 2R itraconazole the distance is between the carbonyl carbon present in triazol ring and tertiary nitrogen present in second triazol ring. Similarly, the N1-N1 distances in 2S, 4R, 2S isomer of itraconazole is observed between ether oxygen and tertiary nitrogen of triazol ring and between ether oxygen and carbonyl oxygen in case of 2S, 4R, 2R isomer of itraconazole as shown in figure 21. While in case of ketoconazole the feature is absent in R isomer and in case of S isomer the distance is observed between two tertiary nitrogen groups present in imidazole and piperazin rings of

ketoconazole respectively. The difference in the groups computing the distances among the stereoisomers of same drug is due to the rotation of functional groups around the stereo-center. Although, resemblances exist in the presence as well as number of H-bond acceptors essential for inhibitory activity of CYP3A4 inhibitors but comparison of distances between two hydrogen bond acceptors from various studies is difficult. It is either due to limited availability of previous GRIND studies on CYP3A4 inhibitors or the distances vary as different studies selected structurally diverse compounds to build the GRIND model as in case of a study by Shityakov, *et al*, 2014 [74]. Another reason for variation in number of hydrogen bond acceptors and their distance is the promiscuous nature of CYP3A4 binding site, which in previous studies is reported to be having multiple overlapping binding sites, large binding site and its ability to accommodate more than one compound at a time [41, 105].

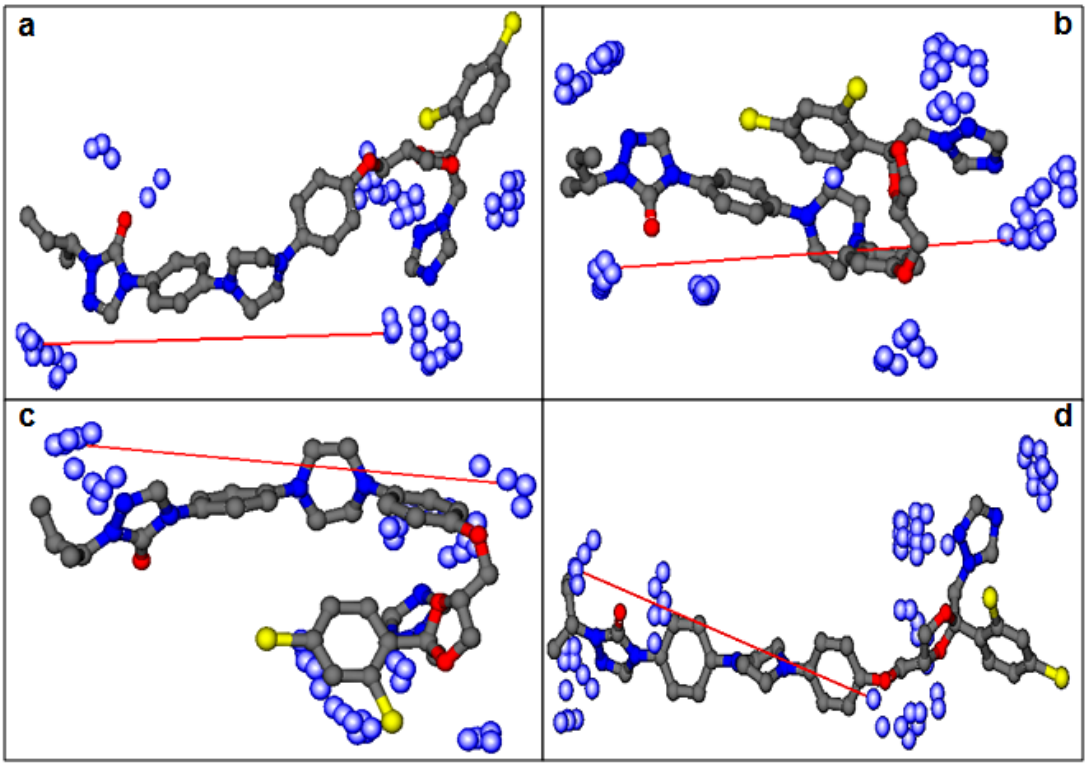


**Figure 21:** N1-N1 distance among different groups in four stereoisomers of itraconazole are illustrated in the above figure where a and b are 2R, 4S, 2S and 2R, 4S, 2R isomers respectively while c and d are 2S, 4R, 2S and 2S, 4R, 2R isomer of itraconazole respectively.

Furthermore, DRY-N1 correlogram demonstrates that a hydrophobic group at a distance of 13.20-13.60Å from a hydrogen bond acceptor group also has positive contribution in the potency of CYP3A4 inhibitors. It is also a differentiating feature between R and S isomers of itraconazole and ketoconazole as it is more pronounced feature in S isomeric form as compared to R in these drugs. This feature represents the distance between tertiary nitrogen acting as hydrogen bond acceptor present in 1,2,4-triazol-1-ylmethyl group while 1,2,4-triazol-5-one act as hydrophobic region which is likely due to the presence of butyl side chain on nitrogen of the triazol ring as shown in figure 22(b). In case of S ketoconazole the oxygen present in 1, 3-dioxolan act as hydrogen bond acceptor while piperazin ring act as hydrophobic region. Likewise N1-TIP distance that is 18.40-18.80Å also contributes positively in the activity of inhibitors and it also differentiates between R and S stereoisomers of ketoconazole and itraconazole. In S isomer of ketoconazole the distance is between oxygen of dioxolan group as hydrogen bond acceptor and terminal ethanone as TIP region while this feature is absent in R isomer as shown in figure 22(c). Similar N1-TIP distance was observed in a study by Cianchetta, *et al*, in which N1-TIP distance was observed to be 19.5Å that is quite close to the distance observed in present study. TIP-TIP correlogram elaborate that that distance between two shape based descriptors at a distance of 20.00-20.40Å contributes positively in the inhibitory potency while the TIP-TIP nodes at a distance of 14.8-15.20Å contributes negatively in the activity of CYP3A4 inhibitors as shown in figure 22(d) [77].

The DRY-TIP nodes about 16.00-16.40Å apart are demonstrated to be contributing positively in inhibitory potency of CYP3A4 inhibitors shown in figure 22(f). The distance between DRY-TIP is also known from previous study by Cianchetta, *et al*, in 2006 to be having a distance of 16.50Å which is quite close to the distance obtained in present study. The DRY-TIP descriptors also differentiate between R and S stereoisomers of itraconazole as

this feature is more pronounced in 2S, 4R, 2S isomer in comparison to 2S, 4R, 2R isomer of itraconazole.

Additionally, O-TIP correlogram showed that hydrogen bond donor group at a distance of 4.8-5.2Å from steric hot spot contributes negatively in the overall activity ($IC_{50}$) of CYP3A4 inhibitors. Another negative contributor in the activity of inhibitors is O-N1 regions at a distance of 8.80-9.20Å which is also a differentiating feature between isomers of nor-fluoxetine and reboxetine as it is present in S isomeric forms that are less active as compared to their R isomers that are more active as shown in figure 22(e). Overall present study is strengthening the analysis from previous studies regarding the importance of hydrophobic, hydrogen bond acceptor and shape based descriptors in the activity of CYP3A4 inhibitors [71, 73]. In addition to that the stereoisomeric forms of these compounds and their importance are also analyzed in this study. Summary of important optimal distances obtained from GRIND analysis are given in the following table 4.

**Table 4:** Summary of important selective features present in CYP3A4 stereoisomeric inhibitors

| **Ligand** | **R/S form** | **DRY-DRY** | **TIP-TIP** | **N1-N1** | **DRY-TIP** | **DRY-N1** | **N1-TIP** | **O-TIP** | **O-N1** |
|---|---|---|---|---|---|---|---|---|---|
| | | **Distances** (Å) | | | | | | | |
| **Impact** | | + | + | + | + | + | + | - | - |
| **Ketamine** | R | Nil | Nil | Nil | Nil | Nil | Nil | 4.80-5.20 | Nil |
| | S | Nil | Nil | Nil | Nil | Nil | Nil | 4.80-5.20 | Nil |
| **Ketoconazole** | R | 12.0-12.40 | 20.00-20.40 | Nil | 16.00-16.40 | 13.20-13.60 | Nil | Nil | Nil |
| | S | 12.0-12.40 | 20.00-20.40 | 16.80-17.20 | 16.00-16.40 | 13.20-13.60 | 18.40-18.80 | Nil | Nil |
| **Verapamil** | R | 12.0-12.40 | Nil | Nil | Nil | 13.20-13.60 | Nil | 4.80-5.20 | 8.8-9.20 |
| | S | 12.0-12.40 | Nil | Nil | Nil | 13.20-13.60 | Nil | 4.80-5.20 | 8.8-9.20 |

| | | | | | | | | | |
|---|---|---|---|---|---|---|---|---|---|
| **Itraconazole** | 2R,4S,2R | 12.0-12.40 | 20.00-20.40 | 16.80-17.20 | 16.00-16.40 | 13.20-13.60 | 18.40-18.80 | Nil | 8.8-9.20 |
| | 2R,4S,2S | 12.0-12.40 | 20.00-20.40 | 16.80-17.20 | 16.00-16.40 | 13.20-13.60 | 18.40-18.80 | Nil | Nil |
| | 2S,4R,2R | 12.0-12.40 | 20.00-20.40 | 16.80-17.20 | 16.00-16.40 | 13.20-13.60 | 18.40-18.80 | Nil | Nil |
| | 2S,4R,2S | 12.0-12.40 | 20.00-20.40 | 16.80-17.20 | 16.00-16.40 | 13.20-13.60 | 18.40-18.80 | Nil | 8.8-9.20 |
| **Nor-Fluoxetine** | R | Nil | Nil | Nil | Nil | 13.20-13.60 | Nil | 4.80-5.20 | Nil |
| | S | Nil | Nil | Nil | Nil | 13.20-13.60 | Nil | 4.80-5.20 | 8.8-9.20 |
| **Fluoxetine** | R | Nil | Nil | Nil | Nil | Nil | Nil | 4.80-5.20 | Nil |
| | S | Nil | Nil | Nil | Nil | Nil | Nil | 4.80-5.20 | Nil |
| **Reboxetine** | R | 12.0-12.40 | Nil | Nil | Nil | Nil | Nil | 4.80-5.20 | Nil |
| | S | 12.0-12.40 | Nil | Nil | Nil | Nil | Nil | 4.80-5.20 | 8.8-9.20 |
| **Dichlobutrazol** | R | 12.0-12.40 | Nil | Nil | Nil | Nil | Nil | 4.80-5.20 | 8.8-9.20 |
| | S | 12.0-12.40 | Nil | Nil | Nil | Nil | Nil | 4.80-5.20 | 8.8-9.20 |

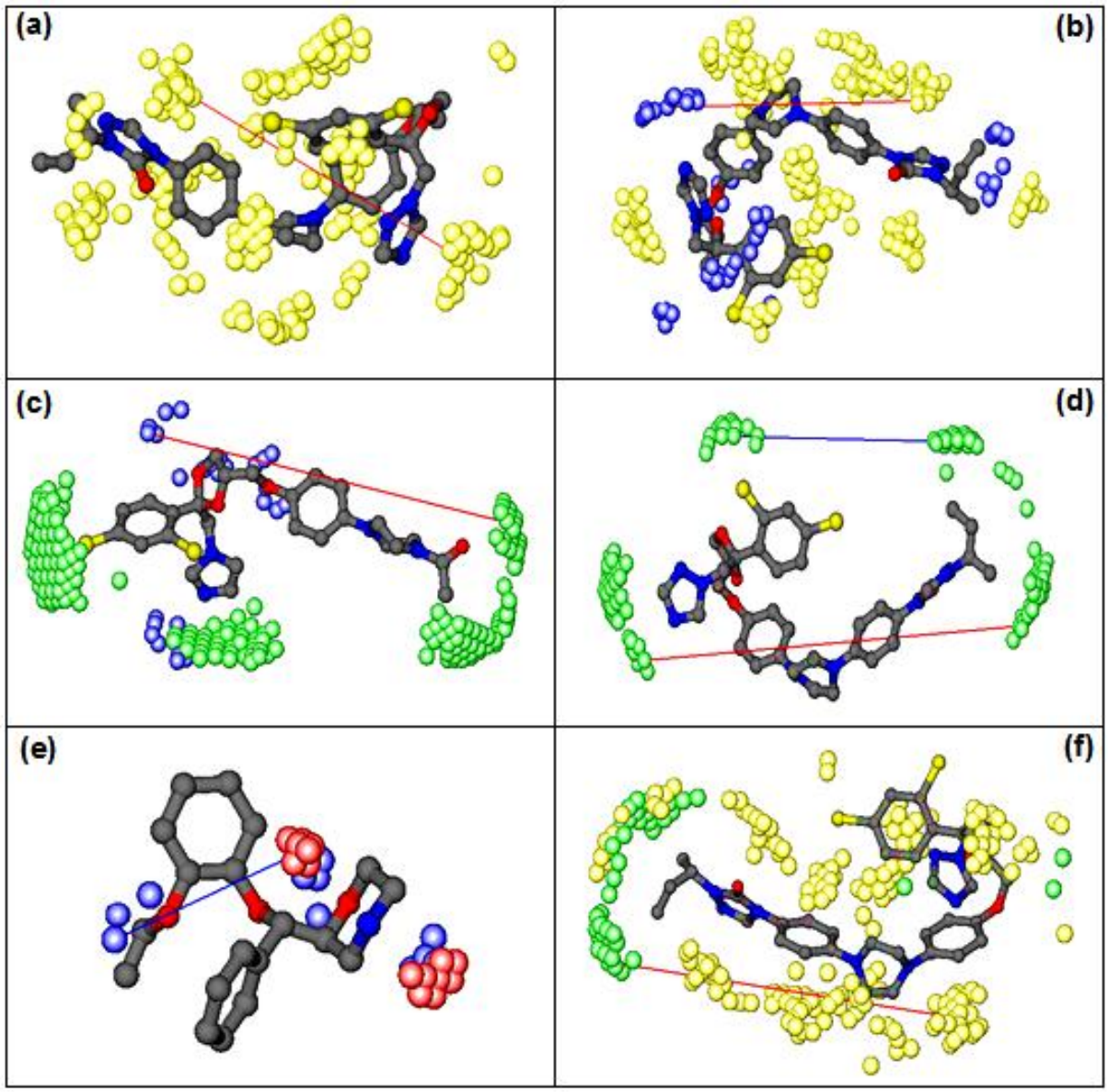


**Figure 22:** (a) Two hydrophobic features (DRY-DRY: yellow contours) at a distance of 12-12.4Å, (b) represents hydrophobic and hydrogen bond acceptor (DRY-N1: yellow and blue contours) regions at an optimal distance of 13.20-13.60Å, (c) showing steric hot spots (green) at a distance of 18.40-18.80Å from hydrogen bond acceptor region (blue) in ketoconazole S isomer, (d) showing two types of distances between steric hot spot (TIP: green contours) the distance is 20.0-20.40Å shown with red line is contributing positively in the activity while the distance 14.8-15.20Å shown in blue is contributing negatively in the activity, (e) depicting distance of 8.80-9.20Å between hydrogen bond donor and hydrogen bond acceptor regions (O-N1: red and blue contours) contributing negatively in the activity in reboxetine S isomer, (f) representing optimal distance of 16.0-16.40Å between hydrophobic and shape based descriptors (DRY-TIP: yellow and green contours).

### 4.4.4. Hotspots Validation:

Validation of the generated hot spots in the current GRIND model was done by importing the protein environments that was CYP3A4 binding cavity in the backstage by using software package Pentacle v 1.06. The model was analyzed for the presence of contours

around complimentary with the amino acids present in that region inside the binding pocket. The amino acid residues that are complimenting the two hydrophobic areas include Phe-108, Phe-215, Phe-220, Phe-57 and pyrrole rings of heme present in the CYP3A4 protein. The distance between heme side chain and phenylalanine cluster is the optimal distance of DRY-N1 descriptors contributing positively toward the inhibitory potency. The positively contributing distance between two hydrogen bond acceptors of 16.80-17.20Å when visualized in the presence of protein also exhibited the presence of hydrogen bond donors in the vicinity. Thus, overall the GRIND model was complimenting the presence of amino acids in the vicinity of important identified contours as shown in the following figure 23.

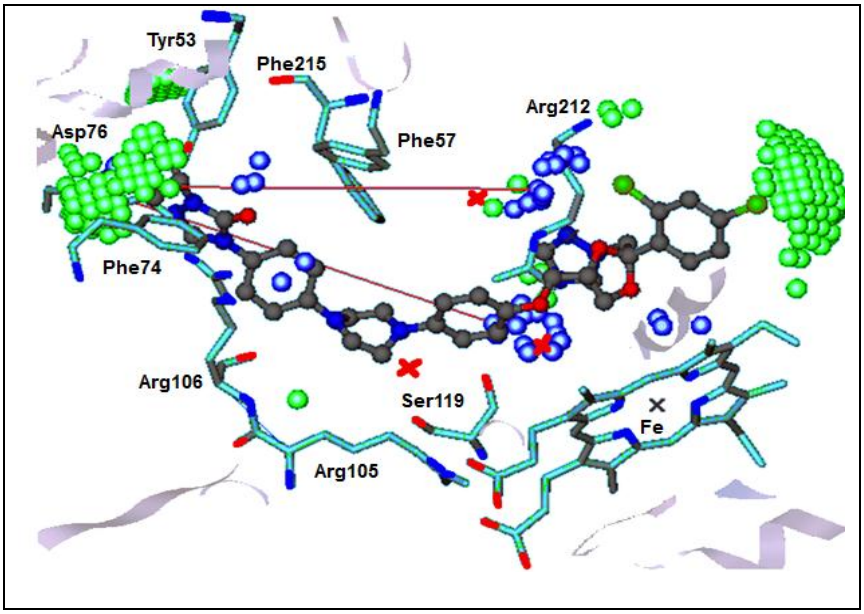


**Figure 23:** N1-N1 and N1-TIP distance are shown in the molecule and the presence of hydrophobic amino acid residues such as Phe74 and Tyr53 in vicinity of shape based descriptor (green contour) and Asp76 as well as the presence of water molecules (represented as red cross) in vicinity of hydrogen bond acceptor descriptor (blue contours) is confirming that the complementary amino acid residues are present in surrounding area of the generated descriptors.

## 4.5. Conclusion:

Current study is application and utilization of rational drug design methodologies that curtails the failure rate of new drug molecules due poor metabolism or drug-drug interaction. According to current paradigm in medicinal chemistry, different stereoisomeric drug might

have different metabolism and interaction potentials and thus, use of enantiopure compounds has advantages over recemates. In current project, the study of interaction of different isomeric forms of drugs with CYP3A4 enzyme is elaborated. Ligand protein interactions by docking and pose analysis of nine pairs of stereoisomeric inhibitors with CYP3A4 enzyme and generation of GRIND 3D QSAR model after selection of best poses was conducted. The GRIND model and interaction studies revealed that the difference in activities among two isomeric forms of same drug is probably due to difference in interaction pattern of these enantiomers with the enzyme CYP3A4. Additionally, our results demonstrates that the isomer that has higher inhibitory potency ($pIC_{50}$) also show better ligand protein interactions as compared to its counterpart stereoisomer. This result is further strengthened by 3D QSAR GRIND models in which the feature that contribute positively in the inhibitory potency of CYP3A4 is also more pronounced in those isomeric forms that have higher $IC_{50}$ values. Specific 3D structural features that were identified to be contributing positively in the inhibition of CYP3A4 include distance between two hydrophobic features (DRY-DRY: yellow contours) that is 12.0 to 12.40Å and distance between two molecular boundaries (TIP-TIP: green contours) that is 20.00 to 20.40Å. The discriminating features between stereoisomers identified include two hydrogen bond acceptors at a distance of 16.80 to 17.20Å (N1-N1: blue contours) from each other,one hydrogen bond acceptor and hydrophobic region (DRY-N1: yellow and blue contours) at a distance of 18.40 to 18.80Å. The distance of about 8.80 to 9.20Å between hydrogen bond donor and hydrogen bond acceptor (O-N1: red and blue contours) is also identified to be discerning between stereoisomeric inhibitors of CYP3A4 although it is a negative contributor in the activity of the inhibitors.

**4.6. Future prospective:**

The outcomes of present investigation can be further elaborated by studying the stability of ligand-protein complexes by molecular dynamic simulations and extending it for more stereoisomeric inhibitors. Nevertheless, these results could aid towards the screening of isomeric forms which are less likely to inhibit CYP3A4 enzyme and thus, chances of toxicity and drug-drug interactions are reduced by administering less toxic enantio-pure drugs to the patients. Overall, the development of *in silico* models for the prediction of drug metabolism and drug-drug interactions would help in improving the understanding of CYP activity (metabolism, inhibition and induction). These models would further aid in exploring major factors involved in CYP inhibition and drug-drug interactions. Moreover, these models can be used as screening tools for the selection of more appropriate drug compounds during the early phases of drug development.

***Chapter 5***

# References


1. Winkler, D.A., *Neural networks in ADME and toxicity prediction.* Drugs of the Future, 2004. **29**(10): p. 1043-1057.
2. Wang, J., L. Urban, and D. Bojanic, *Maximising use of in vitro ADMET tools to predict in vivo bioavailability and safety.* Expert Opinion on Drug Metabolism and Toxicology, 2007. **3**(5): p. 641-665.
3. Xu, C., C.Y.T. Li, and A.N.T. Kong, *Induction of phase I, II and III drug metabolism/transport by xenobiotics.* Archives of Pharmacal Research, 2005. **28**(3): p. 249-268.
4. Bachmann, K.A., *The cytochrome P450 enzymes of hepatic drug metabolism: How are their activities assessed in vivo, and what is their clinical relevance?* American Journal of Therapeutics, 1996. **3**(2): p. 150-171.
5. Tomaszewski, P., et al., *Cytochrome P450 polymorphism - Molecular, metabolic, and pharmacogenetic aspects. III. Influence of CYP genetic polymorphism on population differentiation of drug metabolism phenotype.* Acta Poloniae Pharmaceutica - Drug Research, 2008. **65**(3): p. 319-329.
6. Guengerich, F.P., *Human cytochrome P450 enzymes*, in *Cytochrome P450*. 1995, Springer. p. 473-535.
7. Hakkola, J., et al., *Detection of cytochrome P450 gene expression in human placenta in first trimester of pregnancy.* Biochemical pharmacology, 1996. **52**(2): p. 379-383.
8. Wilkinson, G.R., *Cytochrome P4503A (CYP3A) metabolism: Prediction ofIn Vivo activity in humans.* Journal of pharmacokinetics and biopharmaceutics, 1996. **24**(5): p. 475-490.
9. Wrighton, S.A., M. VandenBranden, and B.J. Ring, *The human drug metabolizing cytochromes P450.* Journal of pharmacokinetics and biopharmaceutics, 1996. **24**(5): p. 461-473.
10. Nelson, D.R., et al., *The P450 superfamily: update on new sequences, gene mapping, accession numbers, early trivial names of enzymes, and nomenclature.* DNA and cell biology, 1993. **12**(1): p. 1-51.
11. Lin, J.H. and A.Y. Lu, *Interindividual variability in inhibition and induction of cytochrome P450 enzymes.* Annual review of pharmacology and toxicology, 2001. **41**(1): p. 535-567.
12. Zhou, S., et al., *Mechanism-based inhibition of cytochrome P450 3A4 by therapeutic drugs.* Clinical Pharmacokinetics, 2005. **44**(3): p. 279-304.
13. Zhou, S.F., et al., *Clinically important drug interactions potentially involving mechanism-based inhibition of cytochrome P450 3A4 and the role of therapeutic drug monitoring.* Therapeutic Drug Monitoring, 2007. **29**(6): p. 687-710.
14. Zanger, U.M. and M. Schwab, *Cytochrome P450 enzymes in drug metabolism: regulation of gene expression, enzyme activities, and impact of genetic variation.* Pharmacology & therapeutics, 2013. **138**(1): p. 103-141.
15. Williams, P.A., et al., *Mammalian microsomal cytochrome P450 monooxygenase: structural adaptations for membrane binding and functional diversity.* Molecular cell, 2000. **5**(1): p. 121-131.
16. Scott, E.E. and J.R. Halpert, *Structures of cytochrome P450 3A4.* Trends in biochemical sciences, 2005. **30**(1): p. 5-7.

17. Raucy, J. and S. Allen, *Recent advances in P450 research.* The pharmacogenomics journal, 2001. **1**(3): p. 178-186.
18. Skopalík, J., P. Anzenbacher, and M. Otyepka, *Flexibility of human cytochromes P450: molecular dynamics reveals differences between CYPs 3A4, 2C9, and 2A6, which correlate with their substrate preferences.* The journal of physical chemistry B, 2008. **112**(27): p. 8165-8173.
19. Kirchmair, J., et al., *Computational prediction of metabolism: sites, products, SAR, P450 enzyme dynamics, and mechanisms.* Journal of chemical information and modeling, 2012. **52**(3): p. 617-648.
20. Peterson, J.A. and S.E. Graham, *A close family resemblance: the importance of structure in understanding cytochromes P450.* Structure, 1998. **6**(9): p. 1079-1085.
21. Pochapsky, T.C., S. Kazanis, and M. Dang, *Conformational plasticity and structure/function relationships in cytochromes P450.* Antioxidants & redox signaling, 2010. **13**(8): p. 1273-1296.
22. Ekroos, M. and T. Sjögren, *Structural basis for ligand promiscuity in cytochrome P450 3A4.* Proceedings of the National Academy of Sciences, 2006. **103**(37): p. 13682-13687.
23. Anzenbacher, P. and E. Anzenbacherova, *Cytochromes P450 and metabolism of xenobiotics.* Cellular and Molecular Life Sciences CMLS, 2001. **58**(5-6): p. 737-747.
24. Kantola, T., K.T. Kivistö, and P.J. Neuvonen, *Erythromycin and verapamil considerably increase serum simvastatin and simvastatin acid concentrations.* Clinical Pharmacology & Therapeutics, 1998. **64**(2): p. 177-182.
25. Ernest, C.S., S.D. Hall, and D.R. Jones, *Mechanism-based inactivation of CYP3A by HIV protease inhibitors.* Journal of Pharmacology and Experimental Therapeutics, 2005. **312**(2): p. 583-591.
26. Zhou, S.-F., *Drugs behave as substrates, inhibitors and inducers of human cytochrome P450 3A4.* Current drug metabolism, 2008. **9**(4): p. 310-322.
27. Obach, R.S., *Inhibition of human cytochrome P450 enzymes by constituents of St. John's Wort, an herbal preparation used in the treatment of depression.* Journal of Pharmacology and Experimental Therapeutics, 2000. **294**(1): p. 88-95.
28. Adams, C.P. and V.V. Brantner, *Estimating the cost of new drug development: is it really $802 million?* Health Affairs, 2006. **25**(2): p. 420-428.
29. Ekins, S., et al., *Predicting drug-drug interactions in silico using pharmacophores: a paradigm for the next millennium.* Pharmacophore Perception, Development and Use in Drug Design, 2000: p. 269-299.
30. Yamashita, F. and M. Hashida, *In silico approaches for predicting ADME properties of drugs.* Drug metabolism and pharmacokinetics, 2004. **19**(5): p. 327-338.
31. van de Waterbeemd, H., *High-throughput and in silico techniques in drug metabolism and pharmacokinetics.* Current opinion in drug discovery & development, 2002. **5**(1): p. 33-43.
32. Butina, D., M.D. Segall, and K. Frankcombe, *Predicting ADME properties in silico: methods and models.* Drug discovery today, 2002. **7**(11): p. S83-S88.
33. Burden, F.R., et al., *Use of automatic relevance determination in QSAR studies using Bayesian neural networks.* Journal of chemical information and computer sciences, 2000. **40**(6): p. 1423-1430.
34. Curtiss, L.A., K. Raghavachari, and J.A. Pople, *Gaussian-2 theory: Use of higher level correlation methods, quadratic configuration interaction geometries, and second-order Mo/ller–Plesset zero-point energies.* The Journal of chemical physics, 1995. **103**(10): p. 4192-4200.

35. Kontijevskis, A., J. Komorowski, and J.E. Wikberg, *Generalized proteochemometric model of multiple cytochrome p450 enzymes and their inhibitors.* Journal of chemical information and modeling, 2008. **48**(9): p. 1840-1850.
36. Wanchana, S., F. Yamashita, and M. Hashida, *QSAR analysis of the inhibition of recombinant CYP 3A4 activity by structurally diverse compounds using a genetic algorithm-combined partial least squares method.* Pharmaceutical research, 2003. **20**(9): p. 1401-1408.
37. Kriegl, J.M., et al., *Multivariate modeling of cytochrome P450 3A4 inhibition.* European journal of pharmaceutical sciences, 2005. **24**(5): p. 451-463.
38. Klingenberg, M., *Pigments of rat liver microsomes.* Archives of biochemistry and biophysics, 1958. **75**(2): p. 376-386.
39. Nelson, D.R., et al., *P450 superfamily: update on new sequences, gene mapping, accession numbers and nomenclature.* Pharmacogenetics and Genomics, 1996. **6**(1): p. 1-42.
40. Shou, M., et al., *Activation of CYP3A4: evidence for the simultaneous binding of two substrates in a cytochrome P450 active site.* Biochemistry, 1994. **33**(21): p. 6450-6455.
41. Schrag, M.L. and L.C. Wienkers, *Covalent alteration of the CYP3A4 active site: evidence for multiple substrate binding domains.* Archives of biochemistry and biophysics, 2001. **391**(1): p. 49-55.
42. De Groot, M.J., *Designing better drugs: predicting cytochrome P450 metabolism.* Drug discovery today, 2006. **11**(13): p. 601-606.
43. Johnson, E.F. and C.D. Stout, *Structural diversity of human xenobiotic-metabolizing cytochrome P450 monooxygenases.* Biochemical and biophysical research communications, 2005. **338**(1): p. 331-336.
44. Yano, J.K., et al., *The structure of human microsomal cytochrome P450 3A4 determined by X-ray crystallography to 2.05-Å resolution.* Journal of Biological Chemistry, 2004. **279**(37): p. 38091-38094.
45. Williams, P.A., et al., *Crystal structures of human cytochrome P450 3A4 bound to metyrapone and progesterone.* Science, 2004. **305**(5684): p. 683-686.
46. Sevrioukova, I.F. and T.L. Poulos, *Structure and mechanism of the complex between cytochrome P4503A4 and ritonavir.* Proceedings of the National Academy of Sciences, 2010. **107**(43): p. 18422-18427.
47. Sevrioukova, I.F. and T.L. Poulos, *Pyridine-Substituted Desoxyritonavir Is a More Potent Inhibitor of Cytochrome P450 3A4 than Ritonavir.* Journal of medicinal chemistry, 2013. **56**(9): p. 3733-3741.
48. Sevrioukova, I.F. and T.L. Poulos, *Structural and mechanistic insights into the interaction of cytochrome P4503A4 with bromoergocryptine, a type I ligand.* Journal of biological chemistry, 2012. **287**(5): p. 3510-3517.
49. Sevrioukova, I.F. and T.L. Poulos, *Interaction of human cytochrome P4503A4 with ritonavir analogs.* Archives of biochemistry and biophysics, 2012. **520**(2): p. 108-116.
50. Sevrioukova, I.F. and T.L. Poulos, *Dissecting Cytochrome P450 3A4–Ligand Interactions Using Ritonavir Analogues.* Biochemistry, 2013. **52**(26): p. 4474-4481.
51. Harlow, G.R. and J.R. Halpert, *Analysis of human cytochrome P450 3A4 cooperativity: construction and characterization of a site-directed mutant that displays hyperbolic steroid hydroxylation kinetics.* Proceedings of the National Academy of Sciences, 1998. **95**(12): p. 6636-6641.

52. He, Y.A., F. Roussel, and J.R. Halpert, *Analysis of homotropic and heterotropic cooperativity of diazepam oxidation by CYP3A4 using site-directed mutagenesis and kinetic modeling.* Archives of biochemistry and biophysics, 2003. **409**(1): p. 92-101.
53. Domanski, T.L., et al., *Phenylalanine and tryptophan scanning mutagenesis of CYP3A4 substrate recognition site residues and effect on substrate oxidation and cooperativity.* Biochemistry, 2001. **40**(34): p. 10150-10160.
54. Atkins, W.M., *Non-Michaelis-Menten kinetics in cytochrome P450-catalyzed reactions.* Annu. Rev. Pharmacol. Toxicol., 2005. **45**: p. 291-310.
55. Szklarz, G.D. and J.R. Halpert, *Molecular modeling of cytochrome P450 3A4.* Journal of computer-aided molecular design, 1997. **11**(3): p. 265-272.
56. Roussel, F., K.K. Khan, and J.R. Halpert, *The importance of SRS-1 residues in catalytic specificity of human cytochrome P450 3A4.* Archives of biochemistry and biophysics, 2000. **374**(2): p. 269-278.
57. Jayakanthan, M., et al., *Analysis of CYP3A4-HIV-1 protease drugs interactions by computational methods for Highly Active Antiretroviral Therapy in HIV/AIDS.* Journal of Molecular Graphics and Modelling, 2010. **28**(5): p. 455-463.
58. Park, H., S. Lee, and J. Suh, *Structural and dynamical basis of broad substrate specificity, catalytic mechanism, and inhibition of cytochrome P450 3A4.* Journal of the American Chemical Society, 2005. **127**(39): p. 13634-13642.
59. Marechal, J.-D., et al., *In silico and in vitro screening for inhibition of cytochrome P450 CYP3A4 by comedications commonly used by patients with cancer.* Drug metabolism and disposition, 2006. **34**(4): p. 534-538.
60. Shimada, T., et al., *Structure− function relationships of inhibition of human cytochromes P450 1A1, 1A2, 1B1, 2C9, and 3A4 by 33 flavonoid derivatives.* Chemical research in toxicology, 2010. **23**(12): p. 1921-1935.
61. Tanaka, T., T. Okuda, and Y. Yamamoto, *Characterization of the CYP3A4 active site by homology modeling.* Chemical & pharmaceutical bulletin, 2004. **52**(7): p. 830-835.
62. Lill, M.A., M. Dobler, and A. Vedani, *Prediction of Small-Molecule Binding to Cytochrome P450 3A4: Flexible Docking Combined with Multidimensional QSAR.* ChemMedChem, 2006. **1**(1): p. 73-81.
63. Dai, D., et al., *Identification of variants of CYP3A4 and characterization of their abilities to metabolize testosterone and chlorpyrifos.* Journal of Pharmacology and Experimental Therapeutics, 2001. **299**(3): p. 825-831.
64. Tanaka, T., T. Okuda, and Y. Yamamoto, *Characterization of the CYP3A4 active site by homology modeling.* Chemical and pharmaceutical bulletin, 2004. **52**(7): p. 830-835.
65. Kapetanovic, I., *Computer-aided drug discovery and development (CADDD): in silico-chemico-biological approach.* Chemico-Biological Interactions, 2008. **171**(2): p. 165-176.
66. Ekins, S., et al., *Three-dimensional-quantitative structure activity relationship analysis of cytochrome P-450 3A4 substrates.* Journal of Pharmacology and Experimental Therapeutics, 1999. **291**(1): p. 424-433.
67. Ekins, S., et al., *Three-and four-dimensional quantitative structure activity relationship analyses of cytochrome P-450 3A4 inhibitors.* Journal of Pharmacology and Experimental Therapeutics, 1999. **290**(1): p. 429-438.
68. Row, E., et al., *Synthesis of 8-geranyloxypsoralen analogues and their evaluation as inhibitors of CYP3A4.* Bioorganic & medicinal chemistry, 2006. **14**(11): p. 3865-3871.

69. Riley, R., et al., *Development of a generalized, quantitative physicochemical model of CYP3A4 inhibition for use in early drug discovery.* Pharmaceutical research, 2001. **18**(5): p. 652-655.
70. Mao, B., et al., *QSAR Modeling of in Vitro Inhibition of Cytochrome P450 3A4*.* Journal of chemical information and modeling, 2006. **46**(5): p. 2125-2134.
71. Roy, K. and P.P. Roy, *Exploring QSARs for binding affinity of azoles with CYP2B and CYP3A enzymes using GFA and G/PLS techniques.* Chemical biology & drug design, 2008. **71**(5): p. 464-473.
72. Schuster, D., et al., *Development and validation of an in silico P450 profiler based on pharmacophore models.* Current drug discovery technologies, 2006. **3**(1): p. 1-48.
73. Ananthula, R.S., S. Gade, and S. Mahmood, *Three-Dimensional Quantitative Structure-Activity Relationship And Comparative Molecular Field Analysis Of Cyp450 Enzyme System Inhibitors.* Pharma Science Monitor, 2013. **4**(2).
74. Shityakov, S., et al., *Three-dimensional quantitative structure–activity relationship and docking studies in a series of anthocyanin derivatives as cytochrome P450 3A4 inhibitors.* Advances and applications in bioinformatics and chemistry: AABC, 2014. **7**: p. 11.
75. Ul-Haq, Z., et al., *A combined 3D-QSAR and docking studies for the In-silico prediction of HIV-protease inhibitors.* Chem Cent J, 2013. **7**(1): p. 88.
76. Cianchetta, G., et al., *A pharmacophore hypothesis for P-glycoprotein substrate recognition using GRIND-based 3D-QSAR.* Journal of medicinal chemistry, 2005. **48**(8): p. 2927-2935.
77. Cianchetta, G., et al., *Molecular interaction fields in ADME and safety.* Molecular Interaction Fields: Applications in Drug Discovery and ADME Prediction, Volume 27, 2006: p. 197-218.
78. Yap, C.W. and Y.Z. Chen, *Prediction of cytochrome P450 3A4, 2D6, and 2C9 inhibitors and substrates by using support vector machines.* Journal of chemical information and modeling, 2005. **45**(4): p. 982-992.
79. Kriegl, J.M., et al., *A support vector machine approach to classify human cytochrome P450 3A4 inhibitors.* Journal of computer-aided molecular design, 2005. **19**(3): p. 189-201.
80. Zuegge, J., et al., *A fast virtual screening filter for cytochrome P450 3A4 inhibition liability of compound libraries.* Quantitative Structure-Activity Relationships, 2002. **21**(3): p. 249-256.
81. Labute, P., et al., *Flexible alignment of small molecules.* Journal of medicinal chemistry, 2001. **44**(10): p. 1483-1490.
82. Wienkers, L.C., et al., *Cytochrome P-450-mediated metabolism of the individual enantiomers of the antidepressant agent reboxetine in human liver microsomes.* Drug metabolism and disposition, 1999. **27**(11): p. 1334-1340.
83. Lamb, D.C., et al., *Differential inhibition of human CYP3A4 and Candida albicans CYP51 with azole antifungal agents.* Chemico-Biological Interactions, 2000. **125**(3): p. 165-175.
84. Dilmaghanian, S., et al., *Enantioselectivity of inhibition of cytochrome P450 3A4 (CYP3A4) by ketoconazole: testosterone and methadone as substrates.* Chirality, 2004. **16**(2): p. 79-85.
85. Wang, Y.-H., D.R. Jones, and S.D. Hall, *Prediction of cytochrome P450 3A inhibition by verapamil enantiomers and their metabolites.* Drug metabolism and disposition, 2004. **32**(2): p. 259-266.
86. Kunze, K.L., et al., *Stereochemical aspects of itraconazole metabolism in vitro and in vivo.* Drug metabolism and disposition, 2006. **34**(4): p. 583-590.

87. Kwan, H.Y. and W. Thormann, *Enantioselective capillary electrophoresis for the assessment of CYP3A4-mediated ketamine demethylation and inhibition in vitro.* Electrophoresis, 2011. **32**(19): p. 2738-2745.
88. Lutz, J.D., et al., *Stereoselective inhibition of CYP2C19 and CYP3A4 by fluoxetine and its metabolite: implications for risk assessment of multiple time-dependent inhibitor systems.* Drug metabolism and disposition, 2013. **41**(12): p. 2056-2065.
89. Lewis, D.F. and Y. Ito, *Human CYPs involved in drug metabolism: structures, substrates and binding affinities.* Expert opinion on drug metabolism & toxicology, 2010. **6**(6): p. 661-674.
90. Jabeen, I., et al., *Structure–activity relationships, ligand efficiency, and lipophilic efficiency profiles of benzophenone-type inhibitors of the multidrug transporter P-glycoprotein.* Journal of medicinal chemistry, 2012. **55**(7): p. 3261-3273.
91. Shultz, M.D., *Improving the plausibility of success with inefficient metrics.* ACS medicinal chemistry letters, 2013. **5**(1): p. 2-5.
92. Jones, G., et al., *Development and validation of a genetic algorithm for flexible docking.* Journal of molecular biology, 1997. **267**(3): p. 727-748.
93. Pastor, M., et al., *GRid-INdependent descriptors (GRIND): a novel class of alignment-independent three-dimensional molecular descriptors.* Journal of medicinal chemistry, 2000. **43**(17): p. 3233-3243.
94. Durán, A., G.C. Martínez, and M. Pastor, *Development and validation of AMANDA, a new algorithm for selecting highly relevant regions in molecular interaction fields.* Journal of chemical information and modeling, 2008. **48**(9): p. 1813-1823.
95. Refsgaard, H.H., et al., *In silico prediction of cytochrome P450 inhibitors.* Drug development research, 2006. **67**(5): p. 417-429.
96. Lewis, D.F., M.N. Jacobs, and M. Dickins, *Compound lipophilicity for substrate binding to human P450s in drug metabolism.* Drug discovery today, 2004. **9**(12): p. 530-537.
97. Mannu, J., P. Jenardhanan, and P.P. Mathur, *A computational study of CYP3A4 mediated drug interaction profiles for anti-HIV drugs.* Journal of molecular modeling, 2011. **17**(8): p. 1847-1854.
98. Teixeira, V.H., V. Ribeiro, and P.J. Martel, *Analysis of binding modes of ligands to multiple conformations of CYP3A4.* Biochimica et Biophysica Acta (BBA)-Proteins and Proteomics, 2010. **1804**(10): p. 2036-2045.
99. He, Y.A., et al., *Identification of three key residues in substrate recognition site 5 of human cytochrome P450 3A4 by cassette and site-directed mutagenesis.* Biochemistry, 1997. **36**(29): p. 8831-8839.
100. Hayes, C., D. Ansbro, and M. Kontoyianni, *Elucidating substrate promiscuity in the human cytochrome 3A4.* Journal of chemical information and modeling, 2014. **54**(3): p. 857-869.
101. Pastor, M., et al., *GRid-INdependent descriptors (GRIND): a novel class of alignment-independent three-dimensional molecular descriptors.* J Med Chem, 2000. **43**(17): p. 3233-43.
102. Smith, D.A., M.J. Ackland, and B.C. Jones, *Properties of cytochrome P450 isoenzymes and their substrates part 2: properties of cytochrome P450 substrates.* Drug discovery today, 1997. **2**(11): p. 479-486.
103. de Groot, M.J. and S. Ekins, *Pharmacophore modeling of cytochromes P450.* Advanced drug delivery reviews, 2002. **54**(3): p. 367-383.
104. Didziapetris, R., et al., *Trainable structure–activity relationship model for virtual screening of CYP3A4 inhibition.* Journal of computer-aided molecular design, 2010. **24**(11): p. 891-906.

105. Kenworthy, K., et al., *CYP3A4 drug interactions: correlation of 10 in vitro probe substrates.* British journal of clinical pharmacology, 1999. **48**: p. 716-727.